

Perforated Patch-Clamp Analysis of the Passive Membrane Properties of Three Classes of Hippocampal Neurons

NELSON SPRUSTON AND DANIEL JOHNSTON

Division of Neuroscience and Section of Neurophysiology, Department of Neurology, Baylor College of Medicine, Houston, Texas 77030

SUMMARY AND CONCLUSIONS

1. Perforated patch-clamp recordings were made from the three major classes of hippocampal neurons in conventional *in vitro* slices prepared from adult guinea pigs. This technique provided experimental estimates of passive membrane properties (input resistance, R_N , and membrane time constant, τ_m) determined in the absence of the leak conductance associated with microelectrode impalement or the washout of cytoplasmic constituents associated with conventional whole-cell recordings.

2. To facilitate comparison of our data with previous results and to determine the passive membrane properties under conditions as physiological as possible, recordings were made at the resting potential, in physiological saline, and without any added blockers of voltage-dependent conductances.

3. Membrane-potential responses to current steps were analyzed, and four criteria were used to identify voltage responses that were the least affected by activation of voltage-dependent conductances. τ_m was estimated from the slowest component (τ_0) of multiexponential fits of responses deemed passive by these criteria. R_N was estimated from the slope of the linear region in the hyperpolarizing direction of the voltage-current relation.

4. It was not possible to measure purely passive membrane properties that were completely independent of membrane potential in any of the three classes of hippocampal neurons. Changing the membrane potential by constant current injection resulted in changes in R_N and τ_0 ; subthreshold depolarization produced an increase, and hyperpolarization a decrease, in both R_N and τ_0 for all three classes of hippocampal neurons.

5. Each of the three classes of hippocampal neurons also displayed a depolarizing "sag" during larger hyperpolarizing voltage transients. To evaluate the effect of the conductances underlying this sag on passive membrane properties, 2–5 mM Cs^+ was added to the physiological saline. Extracellular Cs^+ effectively blocked the sag in all three classes of hippocampal neurons, but the effect of Cs^+ on R_N , τ_0 , and the voltage dependence of these parameters was unique for each class of neurons.

6. CA1 pyramidal neurons had an R_N of 104 ± 10 (SE) M Ω and τ_0 of 28 ± 2 ms at a resting potential of -64 ± 2 mV ($n = 12$). R_N and τ_0 were larger at more depolarized potentials in these neurons, but the addition of Cs^+ to the physiological saline reversed this voltage dependence.

7. CA3 pyramidal neurons had an R_N of 135 ± 8 M Ω and τ_0 of 66 ± 4 ms at a resting potential of -64 ± 1 mV ($n = 14$). R_N and τ_0 were larger at more depolarized potentials in these neurons, and addition of Cs^+ to the physiological saline resulted in an increase in R_N and τ_0 at all potentials without reversing or eliminating the voltage dependence of these parameters.

8. Dentate granule neurons had an R_N of 446 ± 87 M Ω and τ_0 of 43 ± 4 ms at a resting potential of -73 ± 2 mV ($n = 12$). R_N and τ_0 were larger at more depolarized potentials in these neurons, and addition of Cs^+ to the physiological saline had little or no effect on these parameters.

9. Comparison of the passive membrane properties determined by the use of perforated patch-clamp recording to previous estimates from microelectrode recordings revealed that our estimates of R_N are disproportionately large relative to the increased estimate of τ_0 . To determine whether theoretical models predict this result, we investigated the effect of introducing a somatic leak in analytic and numerical models of neurons with passive membranes. In agreement with our experimental data, these models predict that a somatic leak conductance has a greater effect on R_N than τ_0 . These results support the interpretation that differences between the passive membrane properties obtained by the use of patch-clamp and microelectrode recordings are the result of an impalement-induced conductance in the microelectrode recordings. Furthermore, the difference in the effect of a somatic leak on R_N and τ_0 was greater for models having electrotonically longer dendritic cables. The magnitude of the discrepancy in the increased estimates of R_N and τ_0 determined by the use of patch-clamp recordings therefore suggests that hippocampal neurons are not isopotential, even in the steady state.

10. We conclude that for the three major classes of hippocampal neurons, both R_N and τ_0 are larger than previous estimates provided by microelectrode recordings. In addition, our data indicate that membrane properties traditionally considered passive are at least partially influenced by voltage-dependent conductances active near the resting potential in hippocampal neurons. Differences in the effects of Cs^+ on R_N and τ_0 and the voltage dependence of these parameters suggest that the integrative membrane properties of each class of hippocampal neurons are likely to be influenced by unique types, densities, and distributions of voltage-gated ion channels open at or near the resting membrane potential.

INTRODUCTION

The mechanisms by which neurons integrate input from a vast number of synaptic connections on complex dendritic trees intrigued even the earliest neuroscientists (Lorente de N6 1934; Sherrington 1906). With the advent of microelectrode recordings and the application of linear cable theory to neurons (cf. Rall 1977), a large body of work was dedicated to understanding the membrane properties that determine the magnitude, time course, and passive electrotonic decay of membrane-potential responses to activation of voltage- and synaptically activated conductances (Brown et al. 1981a; Carnevale and Johnston 1982; Jack and Redman 1971; Johnston 1981; Redman 1973, 1976). A general finding of all of these studies is that, although synaptic potentials generated in the distal dendrites undergo significant attenuation as they propagate passively in the dendritic tree, the resulting change in membrane po-

tential at the soma is appreciable. As pointed out by many authors, however, one significant source of error affecting the accuracy of the quantitative findings of these studies is the somatic shunt conductance introduced by microelectrode penetration (Barrett and Crill 1974; Clements and Redman 1989; Durand 1984; Durand et al. 1983; Fatt 1957; Iansek and Redman 1973; Ito and Oshima 1965; Jack 1979; Rall 1977; Rose and Vanner 1988; Turner and Schwartzkroin 1983). Indeed, recent modeling of morphological and physiological properties of central neurons has suggested that somatic shunt conductances may result in significant underestimates of the passive membrane properties of neurons (Durand 1984; Fleshman et al. 1988; Stratford et al. 1989). In the present study we have taken advantage of the ability to perform patch-clamp recordings from *in vitro* slices (Blanton et al. 1989; Edwards et al. 1989) to provide measurements of the passive membrane properties of hippocampal neurons in the absence of impalement-induced conductances. We have avoided the washout of cytoplasmic constituents normally associated with whole-cell recordings by including the pore-forming antibiotic nystatin in the pipette to achieve the perforated patch configuration (Horn and Marty 1988; Korn and Horn 1989).

According to linear cable theory (Rall 1977), the passive membrane properties of a neuron, input resistance (R_N), membrane time constant (τ_m), space constant, and electrotonic length of the dendrites, are determined by the specific membrane resistivity, the specific membrane capacitance, and the internal resistivity. We have focused on obtaining accurate estimates of R_N and τ_m for each of the three major classes of hippocampal neurons: CA1 pyramidal neurons, CA3 pyramidal neurons, and dentate granule neurons. Our results suggest that both R_N and τ_m are larger than previously determined with microelectrodes. Furthermore, when these parameters are examined at different membrane potentials, a more complicated picture of the passive membrane properties of hippocampal neurons emerges.

METHODS

Preparation of hippocampal slices

The brains of adult guinea pigs (4–8 wk old; 200–400 g) were removed rapidly (<1 min), bisected longitudinally, and placed in ice-cold physiological saline. Both hippocampi were removed from the brain, placed on a block of agar, and glued at one end to a mounting block for slicing. Slices were cut 400 μm thick with the use of a vibratome (Pelco 101) and then transferred onto a nylon mesh in a Haas-type recording chamber (Medical Systems) under constant perfusion of physiological saline at a rate of ~ 2 ml/min. A second nylon mesh of coarser separation was placed on top of the slices to stabilize them and to ensure that a thin layer of solution perfused the surface. Hippocampi were maintained in ice-cold saline as much as possible throughout the dissection and slicing procedure. Slices were then gradually warmed to a temperature of 32°C for recording and maintained in an environment of warmed humidified 95% O₂-5% CO₂.

Solutions

Bicarbonate-buffered physiological saline (bubbled with 95% O₂-5% CO₂) had the following composition (in mM): 126 NaCl, 3 KCl, 1.25 NaH₂PO₄, 2 MgSO₄, 24 NaHCO₃, 10 dextrose, and 2 CaCl₂. Pipette saline for perforated-patch recording consisted of

the following (in mM): 55 KCl, 70 K₂SO₄, 7 MgCl₂, 10 *N*-2-hydroxyethylpiperazine-*N'*-2-ethanesulfonic acid (HEPES), and 5 dextrose (pH adjusted to 7.2 with KOH).

Perforated patch-clamp recording

Patch-clamp electrodes were constructed by pulling borosilicate glass micropipettes (Boralex, Dynalab) in two stages with the use of a List L/M-3P-A patch-pipette puller. The heat of the second pull was adjusted to yield two virtually identical electrodes with tip diameters of 2–3 μm . The electrodes were lightly heat polished to tip diameters of 1–2 μm with the use of a Narishige microforge and had resistances of 3–6 M Ω in saline.

Perforated patch-clamp recordings were made with the use of a protocol similar to that described previously (Korn and Horn 1989). Electrode tips were filled with pipette saline and backfilled with pipette saline containing 300 $\mu\text{g/ml}$ nystatin (Sigma) in 0.6% dimethyl sulfoxide (DMSO). The solvation of nystatin was facilitated by bath sonication for 1–3 min. Electrodes were positioned perpendicular to the slice and advanced 50–200 μm after entering saline. Gentle outward pressure was provided to the interior of the patch electrode as the electrode entered the saline, and tip resistance was monitored with a -5 -mV step in continuous voltage-clamp mode. A slight increase in tip resistance was detected as the electrode entered the slice, and another brief pulse of outward pressure was used to clear any debris from the tip of the electrode. After advancing the electrode a minimum of 50–100 μm into the slice, subsequent increases in tip resistance were often associated with the detection of action potentials. When the tip resistance increased to 30–50 M Ω , gentle suction was applied to the patch electrode, and current was injected to bring the patch to a negative potential. Seals generally formed gradually over a period of 10–30 s and reached resistances of ~ 0.5 –5 G Ω . Measurements of seal resistance are likely to be underestimates because perforation of the patch usually began before seal resistance had clearly stabilized. Series resistance decreased as nystatin perforated the patch and was usually low enough for bridge-clamp recording (30–100 M Ω) within a few minutes.

All recordings were made with the use of an Axoclamp 2A amplifier operating in bridge mode. Bridge balance was checked frequently because of changes in series resistance occurring as nystatin perforated the patch. Data were filtered at 3,000 Hz and digitized on-line at a rate of 500–2,000 Hz. Data acquisition software was written in Basic-68 and run on a Masscomp 5400 computer.

Determination of passive membrane properties

All data were analyzed on a Masscomp 5700 computer with the use of software written in Basic-68. Voltage responses to steps of current 200–1,000 ms in duration were averaged, those traces that displayed anomalies or asymmetry in the responses to the onset (current-on) and turn-off (current-off) of the current step were rejected. The most common reason for rejecting traces was the presence of large spontaneous synaptic events. Input resistance (R_N) was determined from the slope of voltage-current plots prepared by plotting the steady-state voltage during the current step versus the amplitude of the step. The membrane time constant (τ_m) was estimated from the slowest component (τ_0) of multiexponential fits to the voltage responses (from the onset to the steady state). Because τ_m can only be estimated accurately from passive voltage responses, it was important to use a number of criteria to identify voltage responses with nonpassive components.

Criteria used to identify nonpassive responses

Because we wanted to determine the passive membrane properties under the most physiological conditions possible, no blockers

of voltage-dependent Na^+ or K^+ conductances were included in the bath or the electrode. We used four criteria to identify (and reject) responses that were contaminated by voltage-dependent conductances activated by the current step. 1) Responses were rejected if they did not fall on the linear portion of the voltage-current plot. In most cases, membrane rectification was observed, and the linear region was by convention chosen to be in the hyperpolarizing direction. R_N was determined from the slope of the best regression line through this linear region. 2) Responses were not fit by multiple exponentials if they displayed a "sag," typically characterized by a slow depolarization after the initial hyperpolarizing response to negative current steps (Purpura et al. 1968). 3) Responses were rejected if τ_0 of the current-on and current-off voltage responses were significantly different; a difference of >20% of the average was considered unacceptable. 4) Finally, we assumed that the smallest hyperpolarizing responses were the most likely to be passive. Larger responses were rejected if τ_0 was >20% different from τ_0 of the smallest hyperpolarizing transient. The 20% cut-off values for the latter two criteria were chosen arbitrarily, but they appeared to allow for differences in time constants caused by random fluctuations in the membrane potential although rejecting responses that were clearly asymmetrical or dependent on the size of the current step. Differences in time constants caused by membrane-potential fluctuations could usually be avoided by averaging traces that displayed the least fluctuation. Differences in time constants caused by activation of voltage-dependent conductances, however, were identifiable because they persisted regardless of which traces were averaged.

Conductances that are activated by the current step should be distinguished from those that are normally active at the resting potential. The criteria described above minimize contributions from the former but not the latter. Therefore application of the four criteria provided a functional definition for what are referred to throughout this paper as passive voltage responses. As the results of this study indicate, however, these so-called "passive" voltage responses, in fact, appear to be determined partially by voltage-dependent conductances active at or near the resting membrane potential. For this reason the term "passive membrane properties" is not entirely accurate, but it is nevertheless consistent with its use in previous publications and serves as a convenient means of referring to parameters measured from responses that are influenced the least by voltage-dependent conductances.

Accuracy of time constants

The best multiexponential fit of each of the current-on and current-off voltage transients was determined with the use of the computerized Fourier method, DISCRETE (Provencher 1976). The ability of the data-acquisition and analysis system to determine accurately the time constants of single exponential transients was assessed with the use of parallel resistor-capacitor combinations with time constants of 10–100 ms. A second resistor of 10–100 M Ω was also placed in series to model the access resistance of the perforated patch. Data collected and analyzed exactly as experimental data resulted in fits that were accurate to $\pm 5\%$ of the actual values. With the bridge balanced properly, the time constants determined were not affected by series resistance.

As a test of the ability of DISCRETE to fit multiple exponentials to voltage transients, we fit transients with up to three exponentials generated by an analytic model of a cable with a lumped soma (see APPENDIX). DISCRETE was able to extract the time constants to an accuracy of $\pm 0.5\%$, over a range of time constants of 0.5–50 ms. This method was dependent, however, on the time step in the data. Accuracy decreased for time constants approaching the time step.

Although the slowest membrane time constant was consistent among different voltage responses from any given neuron, a great

deal of variability was observed in the higher order exponentials. This is likely to result from noise in the recordings, the small amplitude of the faster exponential components, and the relatively slow digitization rate (500–2,000 Hz) required for the on-line digitization of traces as long as 2 s in duration. Because the higher order exponentials were difficult to resolve with our methods, they were not analyzed in this study. Nevertheless, we are confident that we can determine τ_0 with an accuracy of at least $\pm 5\%$.

Analytic and numerical models

Analytic models were computed with the use of *Mathematica*, running on a NeXT computer (68030 microprocessor; NeXTstep 2.0; Mach, UNIX). This program provided a useful environment for solving the cable equations derived for a uniform equivalent cylinder attached to a soma with a variable leak conductance. These equations are described in detail in the APPENDIX.

Numerical models were computed with the use of CABLE running on a Solbourne Series 5 computer (Sun-4 compatible SPARC station; Sun OS/SMP 4.0). This program uses a modification of the Crank-Nicholson method for implicitly solving the cable equations for neurons with arbitrary branching geometries (Hines 1989). Details of the models constructed with CABLE are provided in the APPENDIX.

Statistics

A number of statistical tests were employed in this study, including two-tailed paired sample *t* tests, one- and two-factor analyses of variance (ANOVA), and Tukey's test for multiple comparisons. A significance level of $P < 0.05$ was chosen for all statistical comparisons. All values cited in the text are mean \pm SE.

RESULTS

Passive membrane properties were determined from a total of 38 hippocampal neurons: 12 from area CA1, 14 from area CA3, and 12 from the suprapyramidal blade of the dentate gyrus. Only those responses that could be functionally defined as passive by the criteria outlined in METHODS were analyzed to determine R_N and τ_0 . Although these criteria minimize errors introduced by voltage-dependent conductances activated by the current step, they do not rule out the possibility that some voltage-dependent conductances are active in the steady state at the resting membrane potential. To determine whether these conductances could provide significant contributions to the passive membrane properties of hippocampal neurons, we also measured R_N and τ_0 at a second membrane potential, either hyperpolarized or depolarized from the resting potential. If voltage-dependent conductances do contribute to the passive membrane properties, then it would be expected that changing the membrane potential would alter the R_N and τ_0 values measured. This, in fact, proved to be the case.

All three classes of hippocampal neurons displayed a sag in some of the voltage responses. The nature of the sag, however, was unique for each class of hippocampal neurons. The effect of this sag on the passive membrane properties of all three classes of hippocampal neurons was determined by adding 2–5 mM Cs^+ to the bath, which has been shown to block the sag in a number of cell types, including hippocampal neurons (DiFrancesco 1982; DiFrancesco et

al. 1986; DiFrancesco and Ojeda 1980; Hagiwara et al. 1976; Halliwell and Adams 1982; Spain et al. 1987).

The results of our analyses of the passive membrane properties of CA1 pyramidal neurons, CA3 pyramidal neurons, and dentate granule neurons are described in the following three sections. The final section describes a theoretical analysis of the effects of a somatic leak conductance on the passive membrane properties of model neurons.

Table 1 provides a summary of the data from all three cell types, with R_N and τ_0 at resting, hyperpolarized, and depolarized potentials shown in the left three columns, and the same parameters in the presence of Cs^+ in the right three columns. A graphic comparison of the data from each of the three classes of hippocampal neurons is given in Fig. 1.

CA1 pyramidal neurons

PASSIVE MEMBRANE PROPERTIES OF CA1 NEURONS AT THE RESTING POTENTIAL. In CA1 neurons a prominent sag was present in most voltage responses to both hyperpolarizing and depolarizing current steps, indicating that voltage-dependent conductances were activated by the current step. Voltage responses smaller than ~ 5 mV, however, did not display a noticeable sag and frequently met the other criteria for passive responses (see METHODS). With the use of these passive voltage transients for analysis, the 12 CA1 neurons studied had an R_N of 104 ± 10 M Ω and a τ_0 of 28 ± 2 ms at a resting potential of -64 ± 2 mV.

VOLTAGE DEPENDENCE OF THE PASSIVE MEMBRANE PROPERTIES OF CA1 NEURONS. To determine whether voltage-dependent conductances active in the steady state at the resting membrane potential contribute to the passive membrane properties of CA1 neurons, we measured R_N and τ_0 at a second membrane potential near the resting potential in 8 of the 12 cells studied. Results from one such neuron are shown in Fig. 2. This cell had an R_N of 140 M Ω and a τ_0 of 27 ms at a resting potential of -66 mV (Fig. 2B1). When this cell was hyperpolarized to a membrane potential of -78 mV, R_N decreased to 125 M Ω with a concomitant de-

crease in τ_0 to 22 ms (Fig. 2B2). In each of the eight CA1 neurons studied, both R_N and τ_0 were larger at the more depolarized potentials. Over the small voltage range examined (5–13 mV from the resting potential), these differences were statistically significant (paired t tests, $t = 4.52$ and 4.07 for R_N and τ_0 , respectively). This sensitivity of R_N and τ_0 to membrane potential suggests that these parameters are determined at least in part by voltage-dependent conductances active at or near the resting membrane potential.

EFFECT OF EXTRACELLULAR Cs^+ ON THE PASSIVE MEMBRANE PROPERTIES OF CA1 NEURONS. The prominent sag present in voltage responses larger than ~ 5 mV was characterized by a slow depolarization that followed the initial hyperpolarizing response to negative current steps, as well as a slow hyperpolarization that followed the depolarizing response to positive current steps (Fig. 2A). The resulting voltage responses to current steps near the resting potential were therefore roughly symmetrical in the current-on and current-off responses. This sag could be completely blocked by adding 2–5 mM CsCl to the bath (Fig. 3A). The symmetry of the sag, as well as its sensitivity to low concentrations of extracellular Cs^+ , are consistent with it being produced by a mixed cation conductance activated by hyperpolarization and reversing at a potential depolarized by the resting potential (Halliwell and Adams 1982; Yanagihara and Irisawa 1980).

To determine whether the Cs^+ -sensitive conductance underlying the sag in CA1 pyramidal neurons provides a significant contribution to the passive membrane properties, R_N and τ_0 were also measured after the addition of 2–5 mM CsCl to the physiological saline in 8 of the 12 CA1 cells studied. The effect of Cs^+ on the same CA1 neuron as in Fig. 2 is shown in Fig. 3. The sag was clearly blocked by 3 mM extracellular Cs^+ (Fig. 3A), resulting in a large increase in R_N and τ_0 (Fig. 3B).

The effect of Cs^+ on passive membrane properties was studied in a total of eight CA1 neurons. Statistical testing of

TABLE 1. Summary of input resistance and time constant values recorded from the 3 major classes of hippocampal neurons at the resting potential and a 2nd membrane potential near V_{rest}

	Physiological Saline			+2–5 mM Cs^+		
	V_{rest}	$-V_m$	$+V_m$	V_{rest}	$-V_m$	$+V_m$
CA1 pyramidal neurons						
V_m , mV	-64 ± 2	-70 ± 2	-60 ± 2	-69 ± 2	-76 ± 2	-67 ± 2
τ_0 , ms	28 ± 2	23 ± 2	33 ± 4	35 ± 3	39 ± 4	35 ± 4
R_N , M Ω	104 ± 10	89 ± 10	116 ± 12	145 ± 18	156 ± 20	144 ± 19
n	12	8	8	8	8	8
CA3 pyramidal neurons						
V_m , mV	-66 ± 1	-69 ± 1	-60 ± 1	-67 ± 2	-70 ± 1	-59 ± 1
τ_0 , ms	66 ± 4	61 ± 4	80 ± 7	90 ± 10	86 ± 10	107 ± 14
R_N , M Ω	135 ± 8	125 ± 6	164 ± 9	158 ± 16	156 ± 19	198 ± 20
n	14	14	14	7	7	7
Dentate granule neurons						
V_m , mV	-74 ± 2	-77 ± 1	-64 ± 1	-73 ± 2	-74 ± 2	-64 ± 2
τ_0 , ms	43 ± 4	42 ± 4	54 ± 5	48 ± 5	47 ± 6	53 ± 5
R_N , M Ω	446 ± 87	440 ± 88	560 ± 110	413 ± 72	417 ± 71	474 ± 88
n	12	12	12	7	7	7

Values are means \pm SE. For each neuron $-V_m$ is the more negative and $+V_m$ the more positive potential at which R_N and τ_0 were determined. V_{rest} falls between $-V_m$ and $+V_m$ because the passive membrane properties were examined hyperpolarized to V_{rest} in some neurons and depolarized to V_{rest} in others. Data are given for R_N and τ_0 determined both in physiological saline and in the presence of 2–5 mM added CsCl.

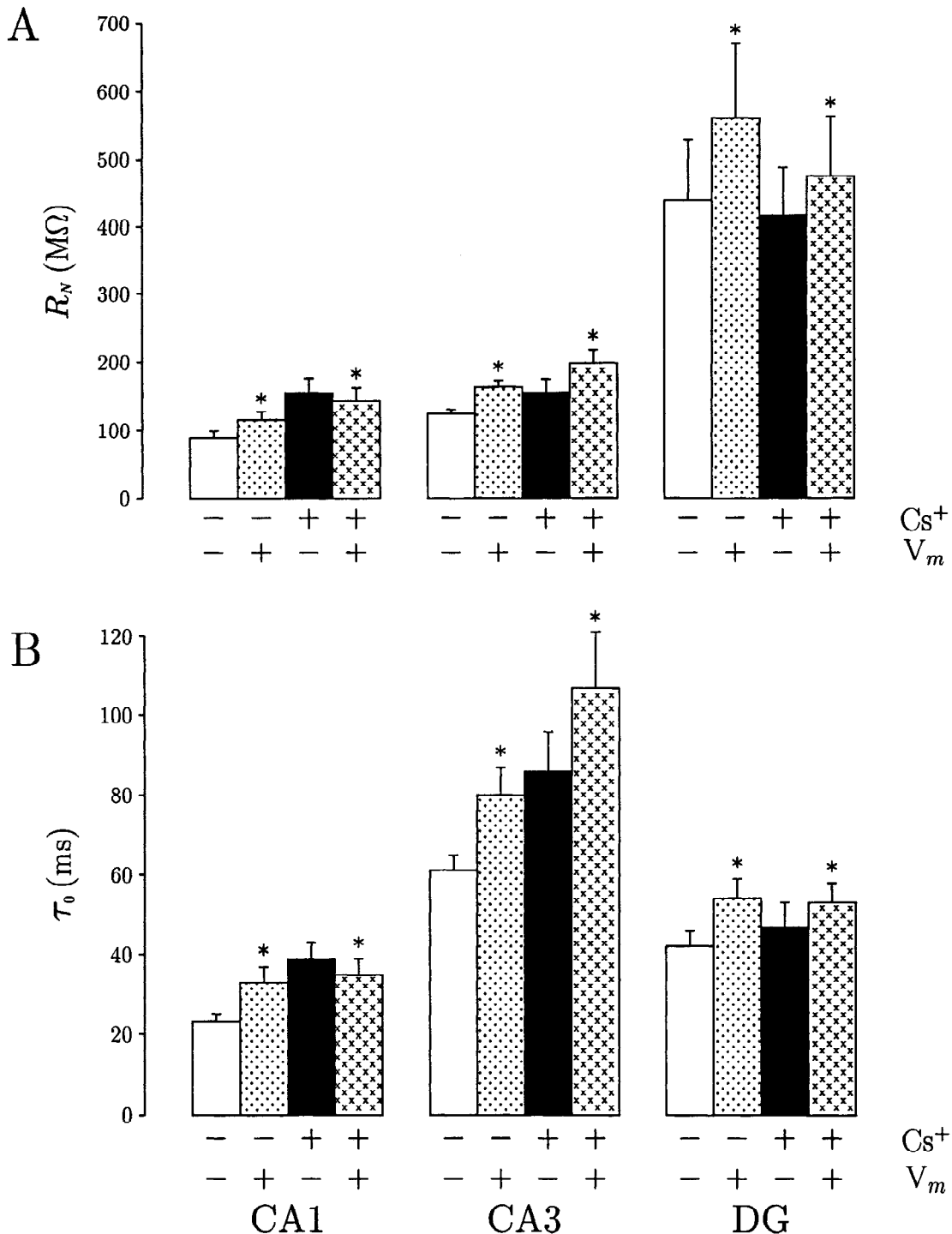


FIG. 1. Summary of the effects of voltage and Cs^+ on the passive membrane properties of hippocampal neurons from areas CA1, CA3, and the dentate gyrus (DG). Input resistance (A; R_N) and time constant (B; τ_0) are plotted at relatively negative ($-V_m$) and positive ($+V_m$) potentials both in the presence ($+Cs^+$) and absence ($-Cs^+$) of 2–5 mM CsCl. All data plotted are means \pm SE. Asterisks above plots of R_N and τ_0 at $+V_m$ indicate a significant difference from the data at $-V_m$ (paired-sample t tests, t values are given in the text).

the apparent increase of R_N and τ_0 in the presence of Cs^+ is complicated by the voltage dependence of these parameters. The apparent effects of two factors (voltage and Cs^+) on these parameters necessitated the use of a two-factor ANOVA. The effect of Cs^+ on both R_N and τ_0 was found to be significant at the membrane potentials studied ($F = 8.80$ and 7.70 for R_N and τ_0 , respectively).

The possibility that the Cs^+ -sensitive conductance underlying the sag is responsible for the observed voltage dependence of R_N and τ_0 was also examined by determining these parameters at two potentials in the presence of Cs^+ . Under these conditions, the voltage dependence of R_N and τ_0 was opposite to that observed in the absence of Cs^+ . In the cell shown in Fig. 3, hyperpolarization in Cs^+ from a

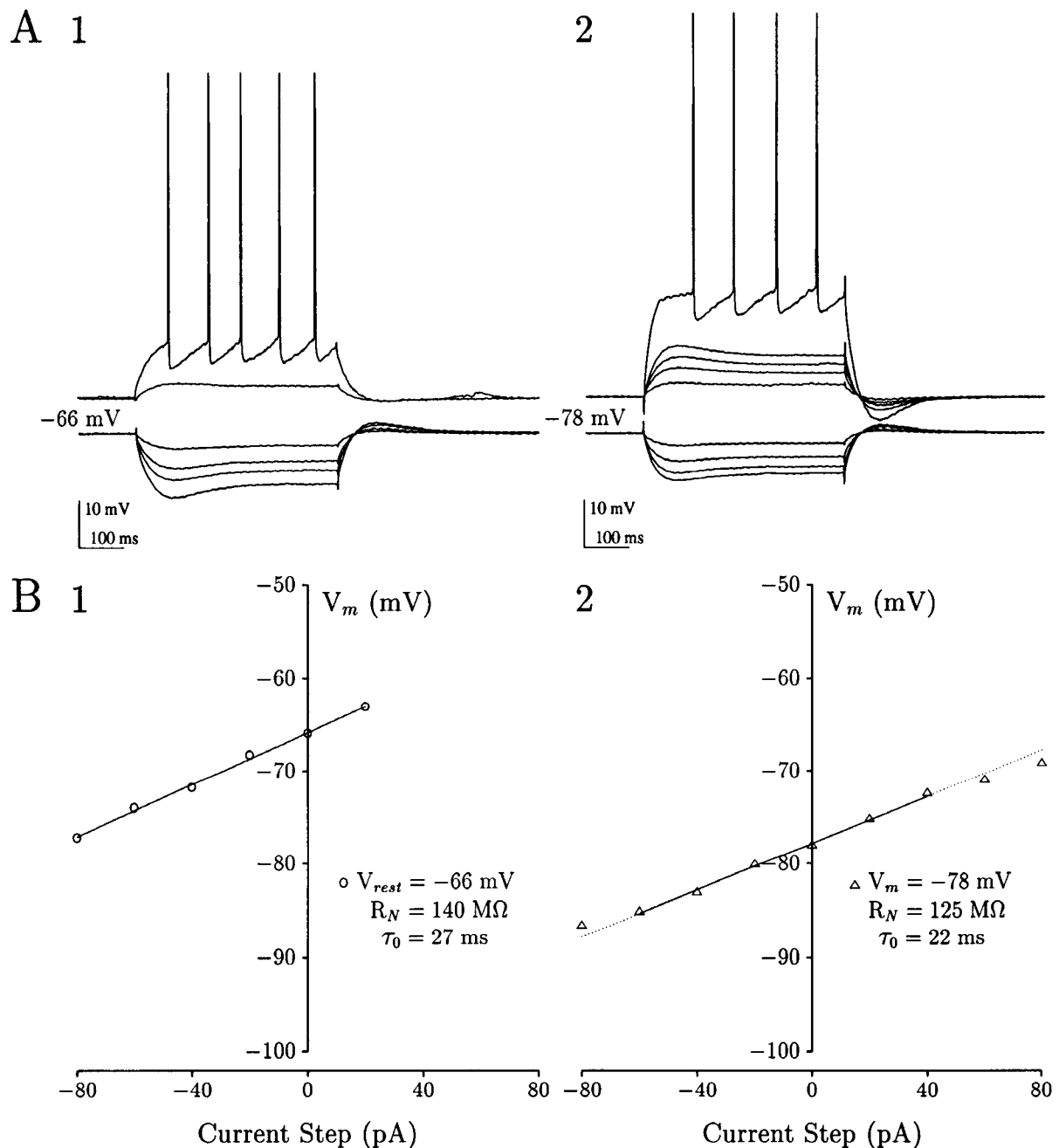


FIG. 2. CA1 pyramidal neurons have smaller R_N and τ_0 at hyperpolarized potentials. *A*: families of voltage responses from a CA1 pyramidal neuron at the resting potential (*A1*) and at a hyperpolarized potential (*A2*, -100-pA current injection). Voltage responses shown are averages of 10–16 traces, with hyperpolarizing and depolarizing responses offset for clarity. Action potentials are single traces in response to +60 pA (*A1*) and +180 pA (*A2*) current steps. *B*: voltage-current plots of responses shown in *A*. R_N values were determined from the linear regressions through the points on the solid lines. The dotted line in *B2* is an extrapolation of the regression line to regions where the points were not considered. τ_0 values were determined from the +20- and -20-pA current steps shown in *A1* and *A2*. Although the responses to some larger current steps fell on the indicated regression lines, τ_0 was not determined from these responses, because of the presence of a sag in the voltage response.

resting potential of -68 mV to a membrane potential of -78 mV resulted in an increase in R_N from 248 to 269 M Ω and an increase in τ_0 from 48 to 54 ms (Fig. 3*B*). In the eight neurons studied, the reversed voltage dependence of R_N and τ_0 in the presence of Cs⁺ was statistically significant (paired *t* tests, *t* = 3.26 and 2.50 for R_N and τ_0 , respectively) over the small voltage range studied (5–15 mV from the

resting potential).¹ This voltage dependence is the opposite of that seen in the absence of Cs⁺, suggesting that indeed

¹ A reversed voltage dependence of R_N and τ_0 was observed in 7 of a total of 8 CA1 neurons studied in the presence of Cs⁺. Measurements were made at 2 potentials both before and after the addition of Cs⁺ in 3 of these 7 neurons, and in all 3 cases a clear reversal of the voltage dependence of R_N and τ_0 was observed after the addition of Cs⁺.

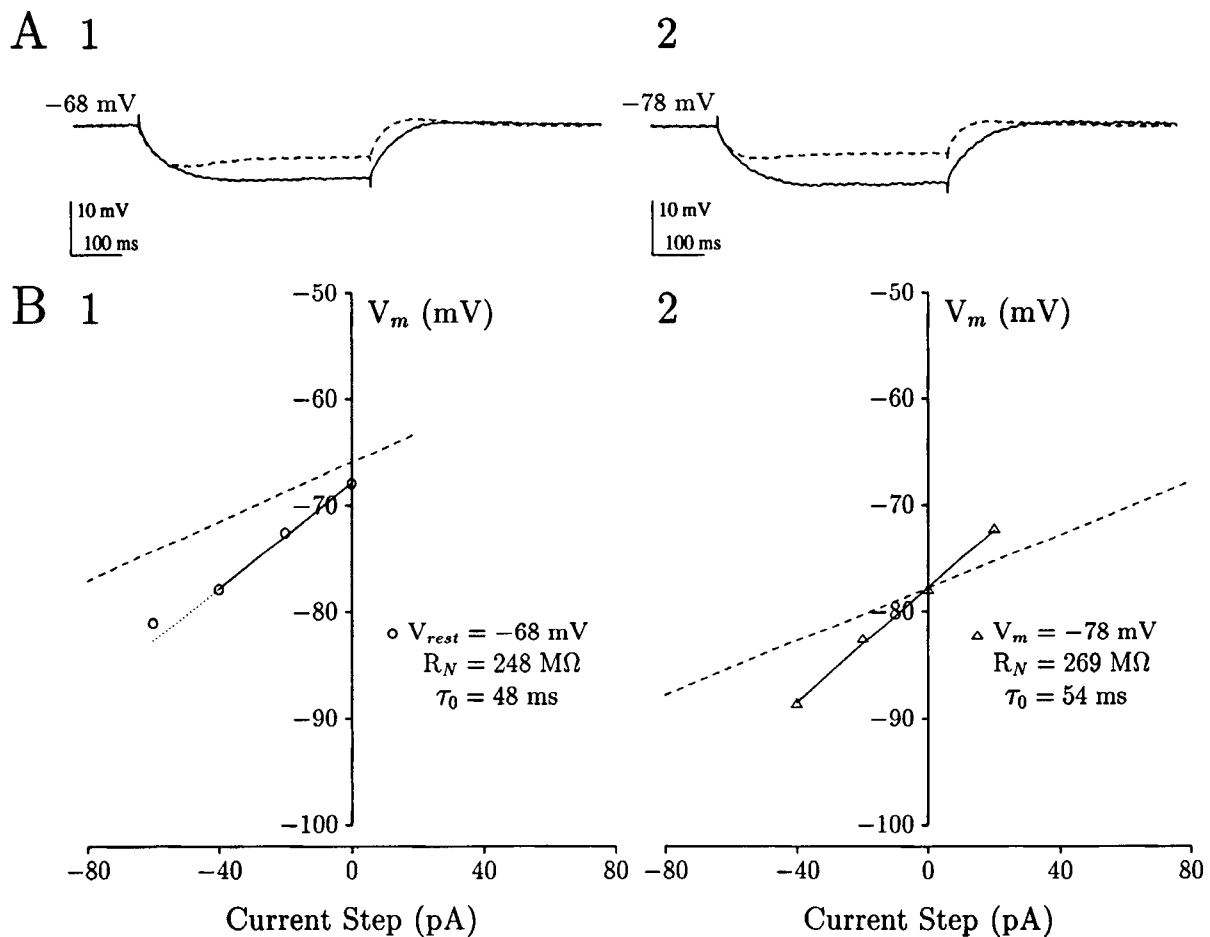


FIG. 3. Extracellular Cs^+ blocks the sag in CA1 pyramidal neurons, causes an increase in R_N and τ_0 , and reverses the voltage dependence of these parameters. Data are from the same cell as Fig. 2. *A*: comparison of the voltage responses to -40 -pA current steps before (---) and after (—) addition of 3 mM CsCl to the bath. Responses are averages of 10 traces from the resting potential (*A1*) and from a hyperpolarized potential (*A2*, -40 -pA current injection). *B*: comparison of the voltage-current plots for responses in the presence (solid lines extrapolated with dotted lines as described in Fig. 2) and absence (dashed lines, data points shown in Fig. 2) of Cs^+ . R_N values were determined from the linear regressions through the points on the solid lines. τ_0 values were determined from the -20 - and -40 -pA steps from the resting potential (*B1*) and the $+20$ - and -20 -pA steps from the hyperpolarized potential (*B2*). Although the -40 -pA response in *B2* fell on the indicated regression line, it was not used for the determination of τ_0 , because dissimilarity in the time constants of the current-on and current-off responses suggested that the response may have a nonpassive component.

the voltage dependence of R_N and τ_0 in physiological saline is mediated by the voltage dependence of a Cs^+ -sensitive conductance, such as the conductance underlying the sag. Although this Cs^+ -sensitive conductance most likely mediates the voltage dependence of R_N and τ_0 , the possibility that other Cs^+ -sensitive conductances also contribute to the voltage dependence of R_N and τ_0 cannot be ruled out. Also, the reversed voltage dependence of R_N and τ_0 in the presence of Cs^+ suggests that Cs^+ -insensitive conductances also provide a voltage-dependent component to the measured values of R_N and τ_0 .

CA3 pyramidal neurons

PASSIVE MEMBRANE PROPERTIES OF CA3 NEURONS AT THE RESTING POTENTIAL. When applying the four criteria described in METHODS to voltage responses from CA3 neurons, we found that only very small responses (<10 mV) could be considered passive, with depolarizing voltage responses be-

ing larger and having slower time constants than hyperpolarizing voltage responses. Analysis of the smallest voltage responses indicated that, at a resting potential of -66 ± 1 mV, CA3 pyramidal neurons had an R_N of 135 ± 8 M Ω and a τ_0 of 66 ± 4 ms ($n = 14$).

VOLTAGE DEPENDENCE OF THE PASSIVE MEMBRANE PROPERTIES OF CA3 NEURONS. The fact that depolarizing current steps resulted in larger voltage responses with slower τ_0 values than responses to hyperpolarizing steps suggested that voltage-dependent conductances active near the resting potential provide a contribution to the passive membrane properties of CA3 neurons. To test this hypothesis, we measured R_N and τ_0 at a second membrane potential near the resting potential in each of the 14 CA3 pyramidal neurons studied. Figure 4 shows an example of one such cell in which R_N increased from 145 to 232 M Ω and τ_0 increased from 95 to 137 ms when the cell was depolarized from a resting potential of -74 mV to a membrane potential of -60 mV. In all of the cells studied, smaller R_N and τ_0 values

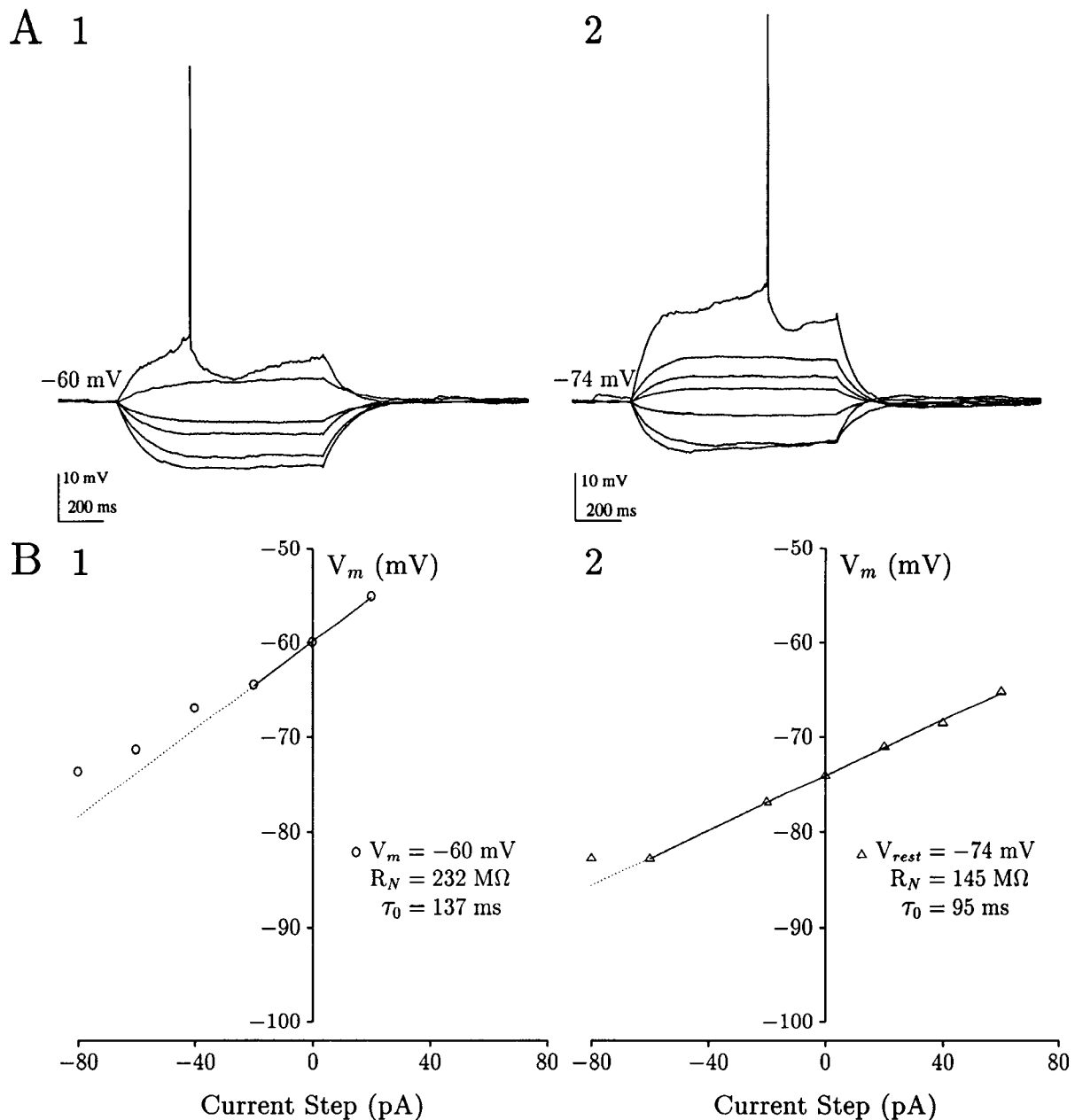


FIG. 4. CA3 pyramidal neurons have smaller R_N and τ_0 values at hyperpolarized potentials. *A*: families of voltage responses at a depolarized potential (*A1*, +80-pA current injection) and at the resting potential (*A2*). Voltage responses shown are averages of 7–23 traces. Action potentials are single traces in response to +60- (*A1*) and +160-pA (*A2*) current steps. *B*: voltage-current plots of responses shown in *A*. R_N values were determined from the linear regressions through the points on the solid lines, and τ_0 values were determined from these linear voltage responses. The dotted lines are extrapolations of the regression lines as described in Fig. 2.

were measured at more hyperpolarized potentials. Over the small voltage range examined (4–14 mV from the resting potential), these differences were statistically significant (paired *t* tests, $t = 7.04$ and 4.77 for R_N and τ_0 , respectively), suggesting that voltage-dependent conductances also contribute to the passive membrane properties of CA3 pyramidal neurons.

EFFECT OF EXTRACELLULAR Cs^+ ON THE PASSIVE MEMBRANE PROPERTIES OF CA3 NEURONS. A sag in hyperpolarizing voltage responses was also observed in some CA3 pyramidal neurons (Fig. 4*A2*). This sag was not as prominent as in

CA1 neurons, however, and appeared to be qualitatively different, because it was only noticeable in larger hyperpolarizing responses and was not as symmetrical as in CA1 neurons. Like the sag in CA1 neurons, the sag in CA3 neurons was sensitive to 2–5 mM extracellular Cs^+ . The properties of the sag in CA3 neurons are consistent with it being caused primarily by an inward-rectifying K^+ current (Constanti and Galvan 1983).

To determine whether the conductance underlying the sag contributed to the passive membrane properties of CA3 neurons and to facilitate comparison of the results among the three classes of neurons studied, the effect of 2–5 mM

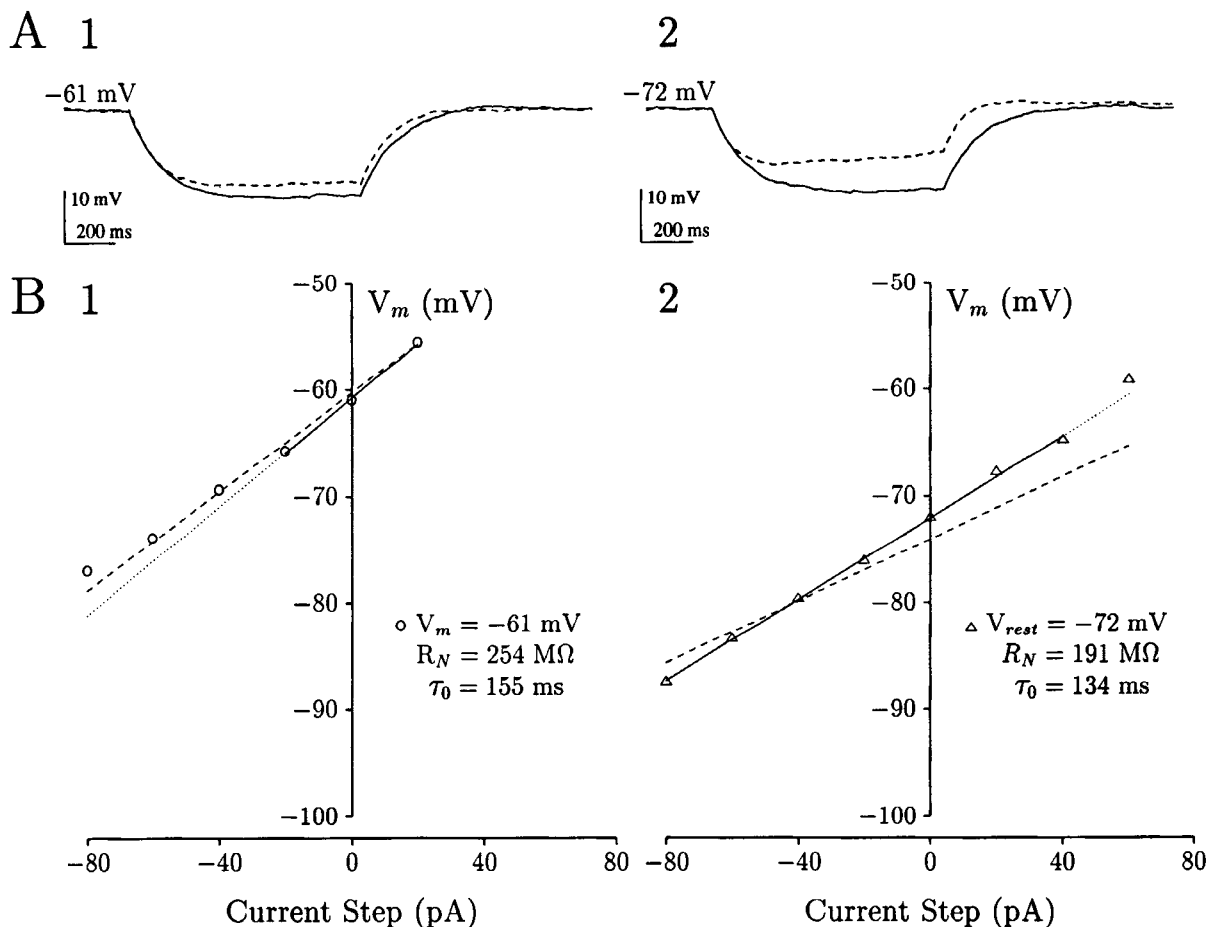


FIG. 5. Extracellular Cs^+ blocks the sag and increases R_N and τ_0 in CA3 pyramidal neurons. Data are from the same cell as Fig. 4. *A*: comparison of the voltage responses to -80-pA current steps before (---) and after (—) addition of 3 mM CsCl to the bath. Responses are averages of 7–13 traces from a depolarized potential (*A1*, $+50\text{-pA}$ current injection) and from the resting potential (*A2*). *B*: comparison of the voltage-current plots for responses in the presence (solid lines extrapolated with dotted lines as described in Fig. 2) and absence (dashed lines, data points shown in Fig. 4) of Cs^+ . R_N values were determined from the linear regressions through the points on the solid lines, and τ_0 values were determined from these linear voltage responses.

Cs^+ on R_N and τ_0 was examined. As shown in Fig. 5 (same neuron as in Fig. 4), Cs^+ completely blocked the sag when added to the physiological saline. In addition, Cs^+ resulted in increases in R_N and τ_0 at both potentials examined. In the seven neurons studied at two potentials both in the absence and presence of Cs^+ , the increase in R_N and τ_0 caused by Cs^+ was statistically significant (2-factor ANOVAs, $F = 6.96$ and 10.54 for R_N and τ_0 , respectively).² These data suggest that a Cs^+ -sensitive conductance is responsible for the sag and that this conductance may be active at the resting potential and provide a contribution to the passive membrane properties of CA3 neurons. The possibility that a Cs^+ -sensitive conductance other than the one underlying the sag is responsible for the increase in R_N and τ_0 , however, cannot be ruled out.

In contrast to the result in CA1 pyramidal neurons, the voltage dependence of R_N and τ_0 in CA3 neurons was not reversed by Cs^+ . In the cell shown in Fig. 5, depolarization in Cs^+ from a resting potential of -72 mV to a membrane

potential of -61 mV resulted in an increase in R_N from 191 to $254 \text{ M}\Omega$ and an increase in τ_0 from 134 to 155 ms (Fig. 5*B*). This voltage dependence is in the same direction as seen in the absence of Cs^+ , suggesting that a Cs^+ -insensitive conductance is at least partially responsible for the observed voltage dependence of R_N and τ_0 under physiological conditions. The voltage dependence of R_N and τ_0 was statistically significant over the small voltage range studied ($8\text{--}14 \text{ mV}$ from the resting potential), both in the absence of Cs^+ (paired t tests, $t = 3.65$ and 4.25 for R_N and τ_0 , respectively) and in the presence of Cs^+ (paired t tests, $t = 2.97$ and 2.97 for R_N and τ_0 , respectively).³

Dentate granule neurons

PASSIVE MEMBRANE PROPERTIES OF DENTATE GRANULE NEURONS AT THE RESTING POTENTIAL. A consistent observation in dentate granule neurons was that voltage responses

² Addition of Cs^+ to the bathing solution resulted in an increase in R_N and τ_0 at all potentials in 6 of 7 CA3 neurons.

³ The voltage dependence of R_N and τ_0 was not altered by Cs^+ in 6 of the 7 CA3 neurons studied. The results from the remaining cell were unclear, because, although the addition of Cs^+ resulted in an increase in both R_N and τ_0 , the voltage dependence of R_N (but not τ_0) was reversed.

tended to be larger and have slower time constants in the depolarizing direction than in the hyperpolarizing direction. Furthermore, voltage responses larger than ~ 10 mV did not meet our criteria for passive responses. With the use of only the small voltage responses that could be considered passive, the 12 dentate granule neurons studied had an R_N of 446 ± 87 M Ω and a τ_0 of 43 ± 4 ms at a resting potential of -74 ± 2 mV.

VOLTAGE DEPENDENCE OF THE PASSIVE MEMBRANE PROPERTIES OF GRANULE NEURONS. To examine the effect of voltage-dependent conductances on R_N and τ_0 in dentate gran-

ule neurons, we determined the passive membrane properties at a second membrane potential near the resting potential. Results from a representative cell are shown in Fig. 6. When this cell was depolarized from a resting potential of -83 mV to a membrane potential of -74 mV, R_N increased from 428 to 580 M Ω with a corresponding increase in τ_0 from 48 to 62 ms. The voltage dependence of R_N and τ_0 was similar in all 12 granule cells studied and was statistically significant (paired t tests, $t = 3.78$ and 5.70 for R_N and τ_0 , respectively) over the small voltage range examined (8–21 mV from the resting potential). This result sug-

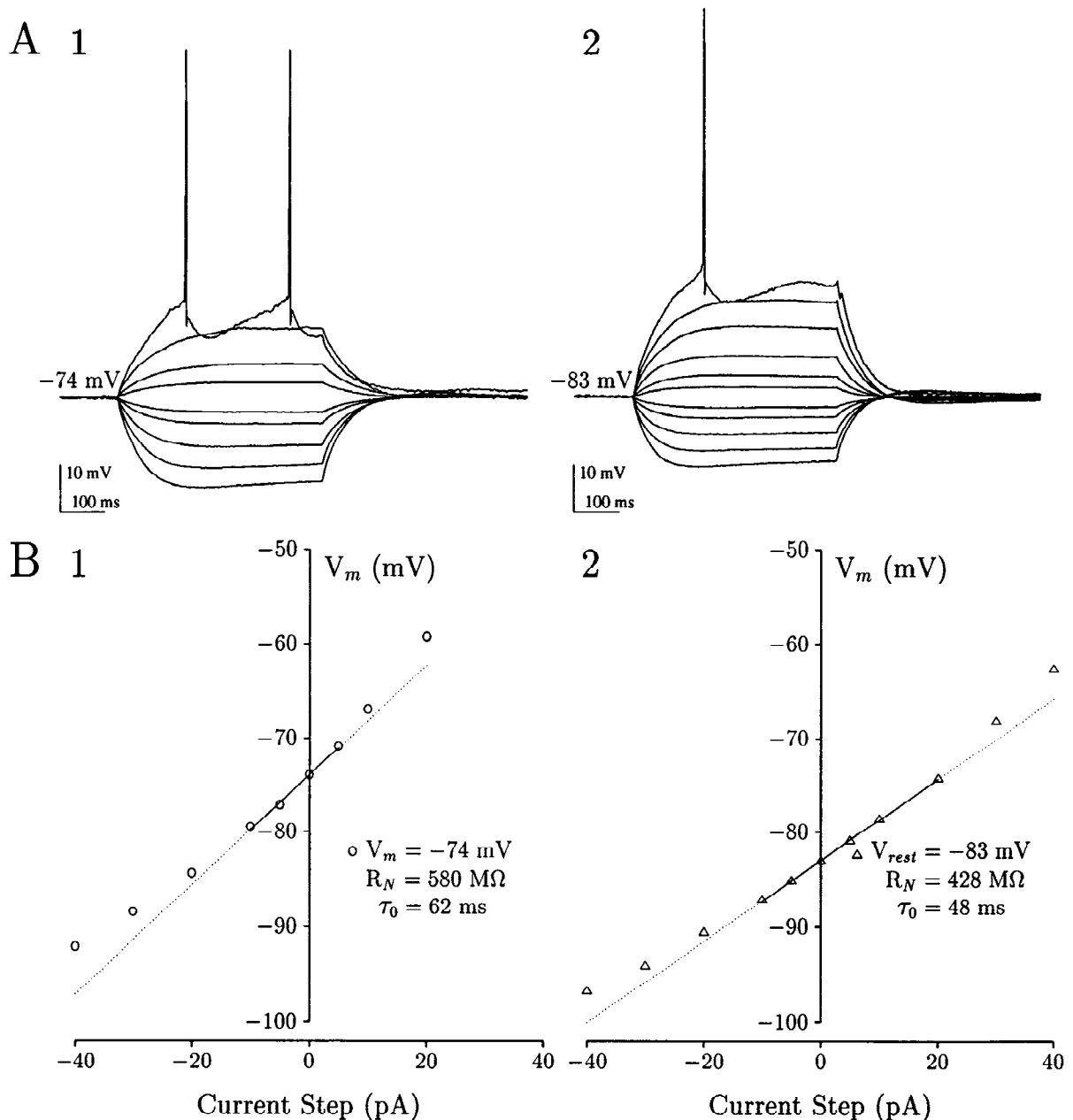


FIG. 6. Dentate granule neurons have smaller R_N and τ_0 values at hyperpolarized potentials. *A*: families of voltage responses at a depolarized potential (*A1*, +20-pA current injection) and at the resting potential (*A2*). Voltage responses shown are averages of 3–19 traces. Action potentials are single traces in response to +30- (*A1*) and +50-pA (*A2*) current steps. *B*: voltage-current plots of responses shown in *A*. R_N values were determined from the linear regressions through the points on the solid lines, and τ_0 values were determined from these linear voltage responses. The dotted lines are extrapolations of the regression lines as described in Fig. 2.

gests that, as is the case in CA1 and CA3 pyramidal neurons, voltage-dependent conductances active near the resting membrane potential contribute to the passive membrane properties of dentate granule neurons.

EFFECT OF EXTRACELLULAR Cs^+ ON THE PASSIVE MEMBRANE PROPERTIES OF GRANULE NEURONS. Dentate granule cells also displayed a sag in hyperpolarizing voltage responses at very negative potentials (see Fig. 6A). Qualitatively, the sag in dentate granule neurons appeared to be more similar to CA3 neurons than CA1 neurons, because it was only activated at very negative potentials and it did not display the

symmetry that was characteristic of the sag in CA1 neurons. Thus the sag in these neurons is likely to be the result of an inward-rectifying K^+ current (Constanti and Galvan 1983).

To determine whether this conductance provided any contribution to the passive membrane properties of dentate granule neurons and to facilitate comparison of the results among all three classes of hippocampal neurons, the effects of 2–5 mM extracellular Cs^+ on R_N and τ_0 were examined in seven granule neurons. In contrast to both CA1 and CA3 pyramidal neurons, Cs^+ appeared to have no effect on R_N

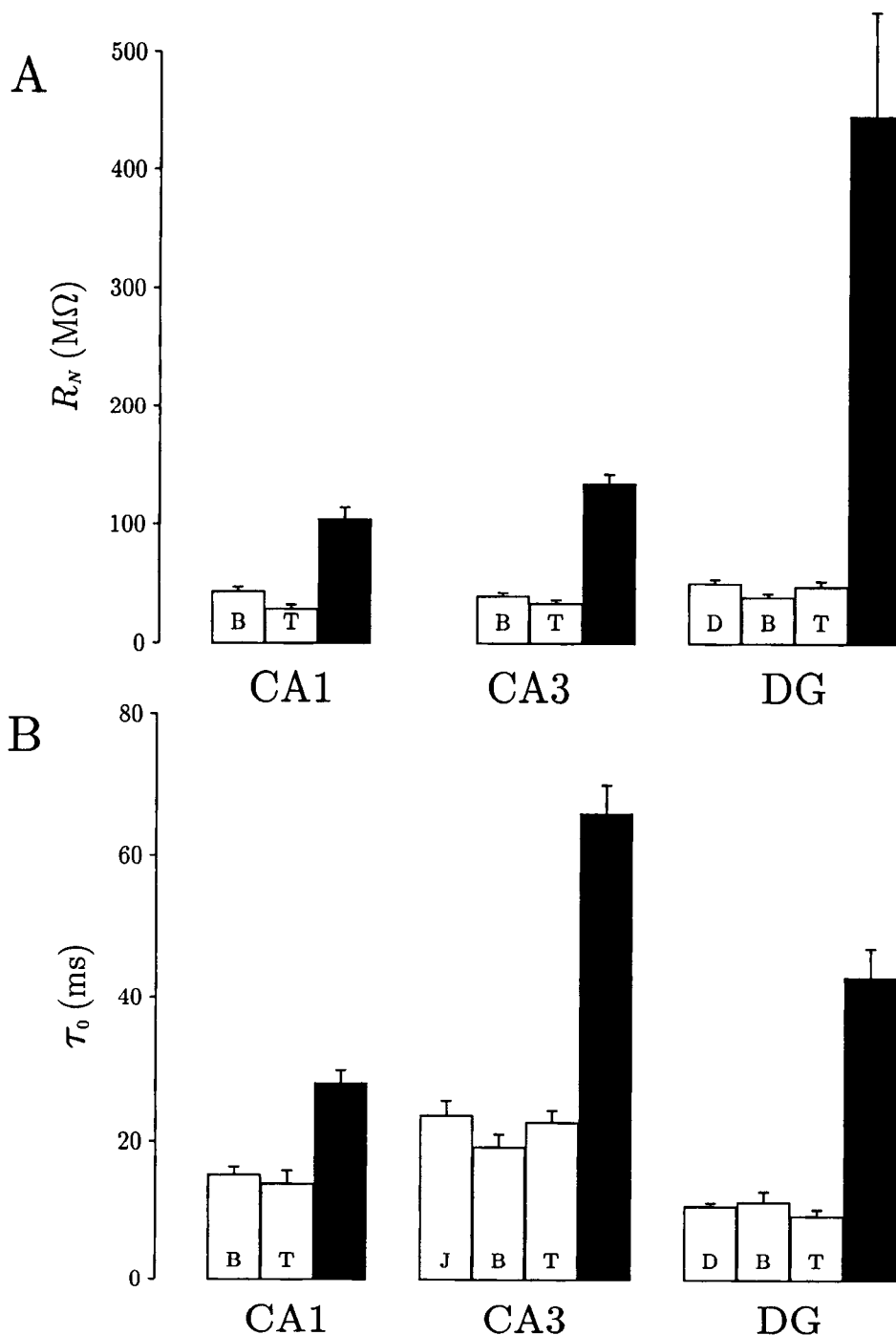


FIG. 7. Comparisons of the input resistance (R_N) and time constant (τ_0) measured by the use of perforated patch-clamp recordings (\blacksquare) and conventional microelectrode recordings (\square). Values for perforated patch-clamp recordings were measured in physiological saline at the resting membrane potential. Microelectrode data (also at the resting potential in physiological saline) are taken from the references indicated by the letter in the bar (B from Brown et al. 1981; T from Turner and Schwartzkroin 1983; D from Durand et al. 1983; J from Johnston 1981).

or τ_0 (2-factor ANOVAs, $F = 0.29$ and 0.25 for R_N and τ_0 , respectively).⁴ The voltage dependence of R_N and τ_0 was statistically significant over the small voltage range studied (9–18 mV from the resting potential), both in the absence of Cs^+ (paired t tests, $t = 2.99$ and 5.03 for R_N and τ_0 , respectively) and in the presence of Cs^+ (paired t tests, $t = 2.94$ and 2.47 for R_N and τ_0 , respectively). The lack of effect of Cs^+ on the voltage dependence of R_N and τ_0 suggests that a Cs^+ -insensitive conductance is responsible for the voltage dependence of the passive membrane properties of dentate granule neurons.

Modeling the effects of a somatic leak on passive membrane properties

Figure 7 compares R_N and τ_0 determined by the use of perforated patch-clamp recording for each of the three major classes of hippocampal neurons with values measured in previous studies with the use of microelectrodes (Brown et al. 1981a; Durand et al. 1983; Johnston 1981; Turner and Schwartzkroin 1983). This figure clearly illustrates the fact that R_N and τ_0 values determined from patch-clamp recordings are larger than the values determined from microelectrode recordings. The simplest explanation for the difference between the data obtained with the two techniques is that microelectrode impalement results in a somatic leak that is prevented by the use of patch-clamp recordings. Figure 7 also demonstrates a result that does not seem to be an intuitive corollary of this explanation: the R_N values observed with patch-clamp recording are much larger relative to the microelectrode data than are the τ_0 values. The microelectrode/patch-clamp ratios for R_N and τ_0 in each class of hippocampal neurons are listed in Table 2.

We tested whether the discrepancy in the effects of a somatic leak on R_N and τ_0 could be accounted for by the existing mathematical formulations for a uniform cable attached to a soma with a lower membrane resistivity (Durand 1984; Iasek and Redman 1973; Kawato 1984; Poznański 1987a,b). We constructed an analytic model of an equivalent cylinder to represent a dendritic tree with uniform membrane resistivity [$R_{m(d)}$], connected to a lumped soma with a variable membrane resistivity [$R_{m(s)}$]. The equations used in the model were derived from previously published equations (see APPENDIX for details), and the value of $R_{m(d)}$ was based on the perforated patch-clamp measurements of τ_0 from dentate granule neurons (assuming $C_m = 1.0 \mu\text{F}/\text{cm}^2$). The model provided analytic solutions for R_N and τ_0 as a function of the somatic leak, which is designated by the term β and is defined as the ratio of the dendritic membrane resistivity to the somatic membrane resistivity [$R_{m(d)}/R_{m(s)}$]. Note that, because the assumption of uniform membrane resistivity (Rall 1969) is clearly not satisfied when a somatic leak is present, τ_0 is only equal to the true membrane time constant (τ_m) in the case where there is no somatic leak (i.e., $\beta = 1$).

Because dentate granule neurons are more likely to be approximated by an equivalent cylinder model than are pyramidal neurons (Turner and Schwartzkroin 1983), we chose the parameters of the model to approximate those of granule neurons. The choice of modeling granule neurons also provided the most stringent test of whether the model can account for the observed differences in the effect of a leak on R_N and τ_0 because this difference is largest for granule neurons (see Table 2). The effect of increasing the leak conductance at the soma [$1/R_{m(s)}$] is shown in Fig. 8. The R_N and τ_0 values are plotted as a function of β and are normalized to the case where there is no somatic leak [i.e., $\beta = 1$; normalized values expressed as $R_N(\beta)/R_N(1)$ and $\tau_0(\beta)/\tau_0(1)$]. The model was found to be in agreement with experimental data, because it predicts that R_N decreases more than τ_0 as the somatic leak is increased. Identical results were also observed with the use of numerical compartmental models of an equivalent cylinder attached to a spherical soma (discussed in APPENDIX). The discrepancy of the effects of a somatic leak on R_N and τ_0 are also apparent in simulations performed by Durand (see Table 2 of Durand 1984).

In the model used to obtain the data plotted in Fig. 8, a single β value accounts well for both the R_N and τ_0 values obtained from microelectrode recordings of dentate granule neurons. However, not all cable models examined were able to do so, and the effects of changing various parameters in the model are shown in Fig. 9. Each pair of plots shows the effect of changing a single parameter in the model while all other parameters are kept constant at the values given in Fig. 8. For each variable that was changed (1 value below and 1 value above that shown in Fig. 8), a new set of curves is illustrated.

Figure 9A demonstrates the effect of changing the length of the cable (l). Increasing values of l resulted in a larger discrepancy in the effects of a somatic leak on R_N and τ_0 . Note that, for the two cable lengths shown, the relative values of β corresponding to the observed microelectrode/patch-clamp ratios for R_N and τ_0 are reversed. This indicates that between these two values there exists an l for which a single β value corresponds to the observed microelectrode/patch-clamp ratios for both R_N and τ_0 ; this is the value shown in Fig. 8. Figure 9, B and C, demonstrates that

TABLE 2. Summary of input resistance and time constant values determined at the resting potential with the use of microelectrode and patch-clamp recordings

	CA1	CA3	DG
R_N , M Ω			
Microelectrode	35.4	36.0	45.2
Patch clamp	104	135	446
Ratio	0.34	0.27	0.10
τ_0 , ms			
Microelectrode	14.6	21.9	10.8
Patch clamp	28	66	43
Ratio	0.52	0.33	0.25

DG, dentate gyrus.

⁴ Of the 7 granule neurons studied, 5 showed no change in the voltage dependence of R_N or τ_0 , 1 cell showed a change only in the voltage dependence of R_N , and the other cell showed a change only in the voltage dependence of τ_0 .

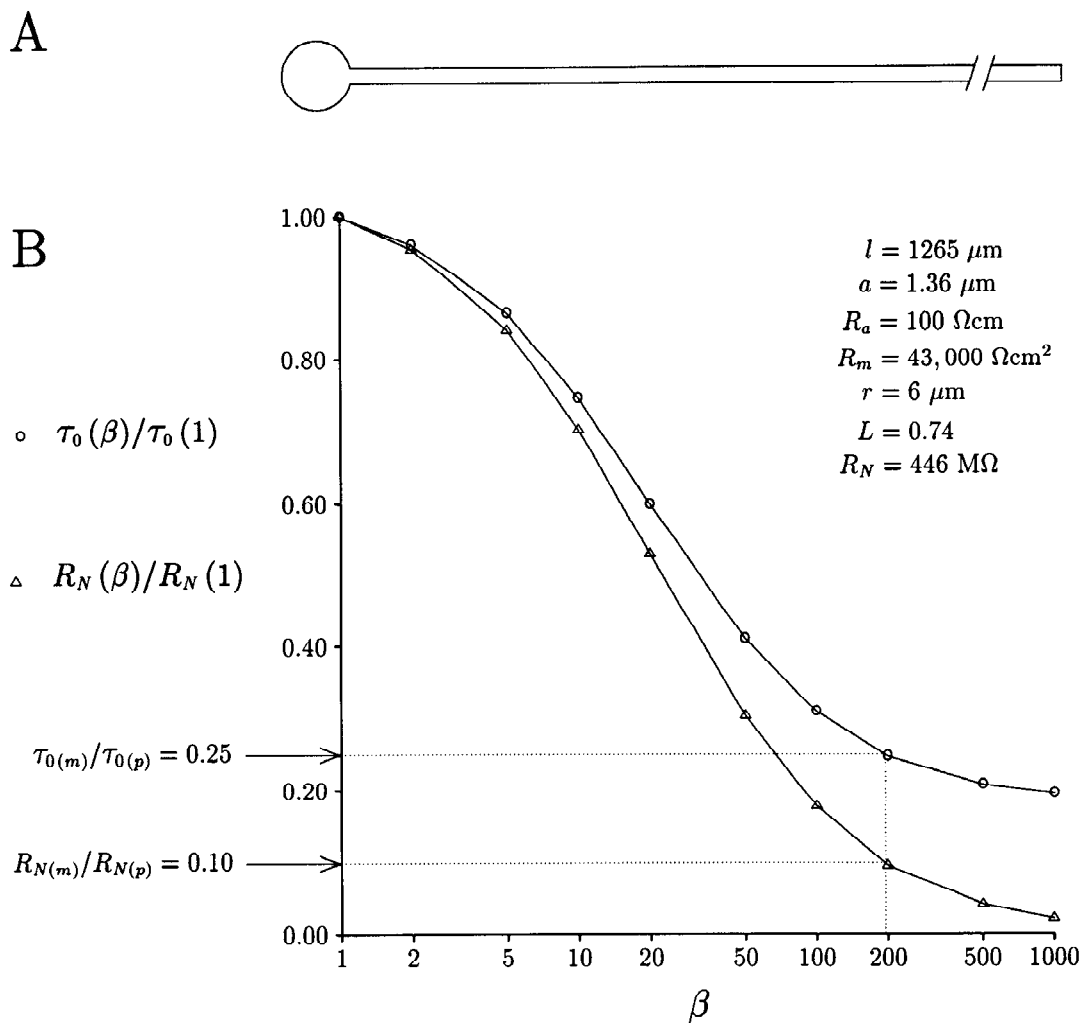


FIG. 8. Modeling results demonstrate that somatic leak conductances have a greater effect on R_N than τ_0 . Analytic solutions of the cable equations modified to account for a variable leak at the soma were used to calculate R_N and τ_0 as a function of somatic leak. The results of these calculations demonstrate that R_N decreases more than τ_0 as the leak at the soma is increased. *A*: schematic diagram of an equivalent cylinder attached to a spherical soma. Soma and cable radii are drawn to scale, but cable length is 10 times shorter than scale. *B*: plot of R_N and τ_0 [normalized to the case where there is no somatic leak; $\beta = 1$; values expressed as $R_N(\beta)/R_N(1)$ and $\tau_0(\beta)/\tau_0(1)$] as a function of β [$R_{m(d)}/R_{m(s)}$]. The dotted lines at $R_N(\beta)/R_N(1) = 0.1$ and $\tau_0(\beta)/\tau_0(1) = 0.25$ indicate the ratios of microelectrode [$R_{N(m)}$ and $\tau_{0(m)}$] to patch-clamp [$R_{N(p)}$ and $\tau_{0(p)}$] data determined experimentally. Both of these ratios can be accounted for by a β value of 195 in this model. The data shown were determined with the use of the equations described in the APPENDIX with the parameters indicated in the top right of the graph.

decreasing the radius (a) or increasing the axial resistivity (R_a) of the cable also resulted in a larger discrepancy in the effect of a somatic leak on R_N and τ_0 and a similar change in the relative β values corresponding to the observed microelectrode/patch-clamp ratios.

Each of these three parameters (l , a , and R_a) affect the electrotonic length (L) of the equivalent cable and the discrepancy in the microelectrode/patch-clamp ratios for R_N and τ_0 . By contrast, altering the dendritic-to-somatic conductance ratio (ρ) by changing the radius of the soma (r) does not affect L and has a negligible effect on the discrepancy in the microelectrode/patch-clamp ratios of R_N and τ_0 (Fig. 9D). For any model in which a single β value could not account for the observed microelectrode/patch-clamp ratios for R_N and τ_0 , altering the size of the soma over a

range of $r = 4\text{--}10 \mu\text{m}$ did not result in a convergence to a single β value.

These findings suggest that L is the critical determinant of the magnitude of the discrepancy in the R_N and τ_0 ratios. Because we were not able to accurately estimate higher order time constants from our data (see METHODS), it was not possible to estimate L with the use of traditional methods (Brown et al. 1981a; Johnston 1981; Rall 1977). L was the critical determinant of the microelectrode/patch-clamp ratios for R_N and τ_0 , however, and it was therefore possible to determine the value of L that resulted in a β that accounted for the observed ratios for R_N and τ_0 . This value was $L = 0.74$ for dentate granule neurons. Although a large number of combinations of l , a , and R_a can yield equivalent cables with an L of 0.74, it was possible to place some con-

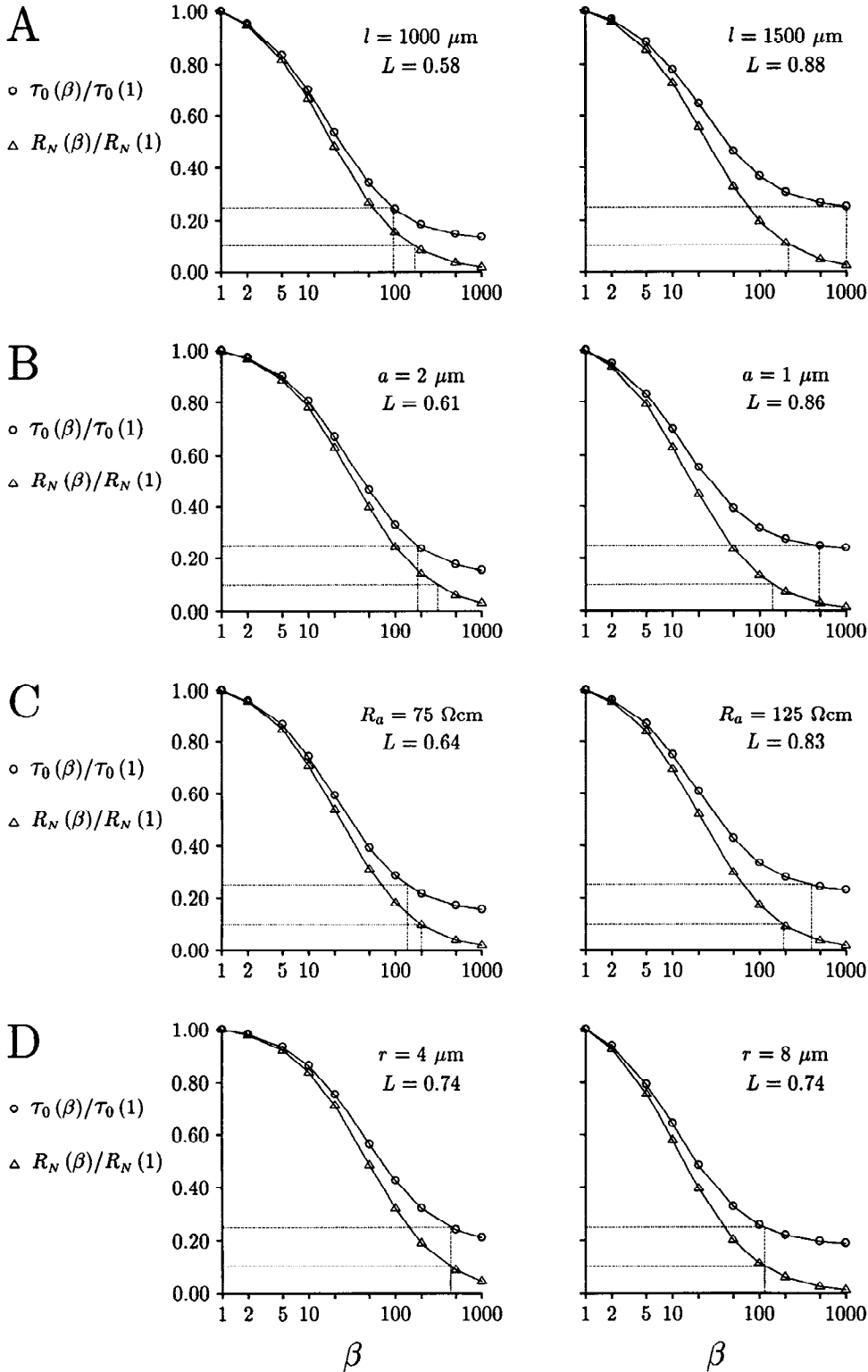


FIG. 9. Electrotonic length of the cable (L) determines the degree of discrepancy between the effects of a somatic leak on R_N and τ_0 . Parameters in the model were systematically varied to determine the effects of each on the result demonstrated in Fig. 8. Parameters that affect L were the only ones that affected the magnitude of the difference between the effects of a somatic leak on R_N and τ_0 on somatic leak. Each pair of plots (*left* and *right*) demonstrate the effect of 1 parameter on the plot of R_N and τ_0 (each normalized to the value at $\beta = 1$) as a function of somatic leak (β). For each plot the values of the varied parameter are indicated in the *top right* of the graph, whereas all other parameters were kept constant at the same values as shown in Fig. 8 ($l = 1,265 \mu\text{m}$, $a = 1.36 \mu\text{m}$, $R_a = 100 \Omega\text{cm}$, and $r = 6 \mu\text{m}$). The parameters l , a , and R_a (*A*, *B*, and *C*, respectively) determine L and have large effects on the difference between the dependences of R_N and τ_0 on β and the relationship between the β values corresponding to the microelectrode/patch-clamp ratios of R_N and τ_0 . By contrast, r (*D*) does not affect L and has no effect on the difference in the dependence of R_N and τ_0 on β .

straints on these parameters on the basis of the measured value of R_N and some known properties of the morphology of granule neurons of the dentate gyrus.

We used the analytic model to calculate R_N for a variety of equivalent cylinders attached to spherical somas. We varied l from a minimum of $300 \mu\text{m}$ to a maximum of

$2,000 \mu\text{m}$. For each value of l we calculated the cable radius (a) required to yield an electrotonic length (L) of 0.74. R_N was then determined for each cable and plotted as a function of l . The minimum value of $300 \mu\text{m}$ was based on published morphology of dentate granule neurons (Clairborne et al. 1990). Cable models with l values smaller than

$\sim 500 \mu\text{m}$, however, had unreasonably high R_N values. Figure 10 shows plots of R_N as a function of l constructed in this way for several values of R_a . For clarity, only those combinations of l , a , and R_a resulting in R_N values of under 2,000 M Ω are plotted. This figure demonstrates that, on the basis of the measured R_N for granule neurons, only a limited range of l , a , and R_a combinations resulted in an R_N of 446 M Ω (the mean value measured for dentate granule neurons). With the use of a lower limit for R_a of 50 Ωcm , an l value of 1,594 μm and a corresponding a value of 1.08 μm yields an R_N of 446 M Ω . This value for R_a was the first used by Rall (1959). We considered this to be a lower limit because measurements of R_a in spinal motoneurons indicate a value of 70 Ωcm (Barrett and Crill 1974), and some authors have suggested that R_a may be much higher than this in central neurons (Shelton 1985; Stratford et al. 1989). With the use of an upper limit of 400 Ωcm , an equivalent cylinder with an R_N of 446 M Ω had an l of 797 μm and a corresponding a of 2.16 μm . This range of values for a (1.08–2.16 μm) is reasonable compared with measurements of the radii of proximal dendrites from horseradish peroxidase-stained dentate granule neurons (Durand et al. 1983).

The total length of the equivalent cylinder can be determined from the lengths of each dendritic segment if the 3/2 power law is assumed to hold at all branch points (Rall 1977). Therefore we used published data on the morphology of granule-neuron dendritic trees (Claiborne et al. 1990) to calculate the approximate length of the equivalent cylinder for granule neurons from the suprapyramidal blade of the dentate gyrus (the region in which all granule-neuron recordings were made). These calculations resulted

in a range of lengths of 366–1,154 μm for 52 dendritic branches measured from three granule neurons. The mean of these lengths ($640 \pm 29 \mu\text{m}$) is somewhat smaller than the length determined for an L of 0.74, R_N of 446 M Ω , and R_a of 100 Ωcm . The shorter lengths measured from anatomic data imply that larger values of R_a are required to yield an L of 0.74. The need for larger values of R_a to account for anatomic and physiological data is consistent with the modeling results of others (Shelton 1985; Stratford et al. 1989).

The data in Fig. 8 were modeled with the use of an R_a value of 100 Ωcm , l of 1,265 μm , and a of 1.36 μm . With the use of these parameters, a single β value of 195 resulted in the observed microelectrode/patch-clamp ratios for both R_N and τ_0 . The β value that accounted for these ratios was independent of the combination of R_a , l , and a used to give an L of 0.74 but is dependent on the radius of the soma (r). We used spherical somata with radii from 4–10 μm to provide a reasonable approximation of the range of surface areas for granule-neuron somata. These surface area estimates are only rough approximations because only two-dimensional data are available and granule-neuron somata appear to be elliptical rather than spherical (Claiborne et al. 1990). The ρ values corresponding to somata of 4 and 10 μm (each attached to cables with $L = 0.74$) were 46 and 7.3, respectively. The β values that accounted for the microelectrode results with the use of the lower and upper limits of somatic surface area were 78 and 447, respectively, and correspond to leak conductances of 21 and 23 nS, respectively. This estimate of microelectrode leak conductance agrees reasonably well with previous estimates, which range

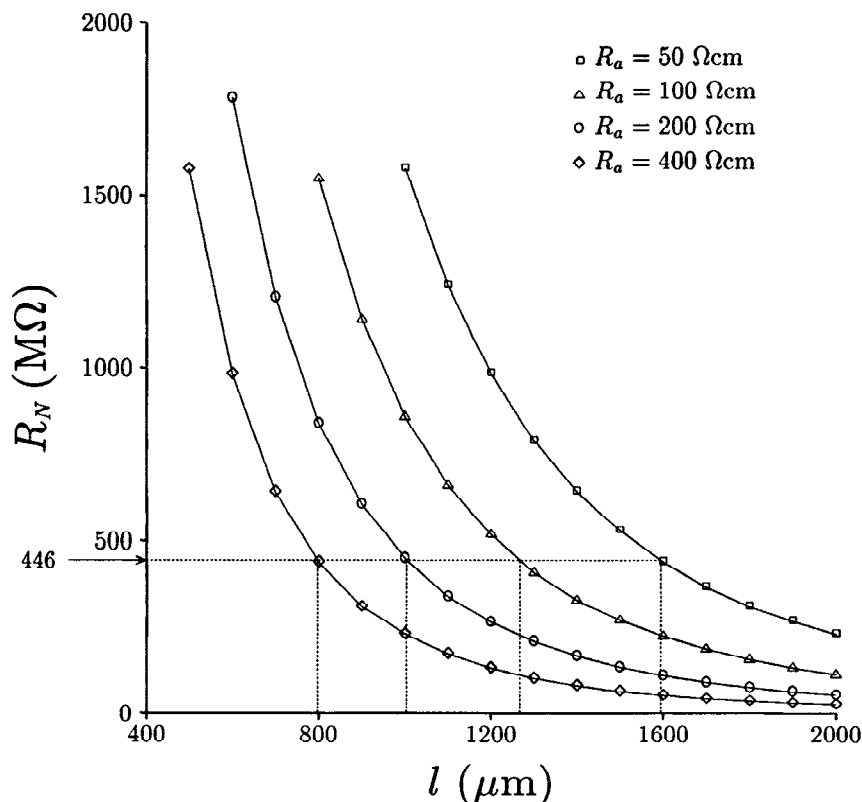


FIG. 10. Physiological measurements of passive membrane properties can be used to place reasonable constraints on the parameters used in an equivalent cylinder model of a typical dentate granule neuron. The length and diameter of the equivalent cable having an electrotonic length (L) of 0.74 can be constrained by the input resistance R_N . R_N is plotted as a function of cable length (l) for cables forced to an L of 0.74 by determining the appropriate cable radius (a). Each of the four curves correspond to different values of R_a as indicated by the key in the top right of the graph. The horizontal dotted line at $R_N = 446 \text{ M}\Omega$ indicates the mean R_N determined by the use of perforated patch-clamp recordings from dentate granule neurons. The vertical dotted lines indicate the l values corresponding to $R_N = 446 \text{ M}\Omega$ for each value of R_a ($l = 797 \mu\text{m}$, $a = 2.16 \mu\text{m}$, $R_a = 400 \Omega\text{cm}$; $l = 1,004 \mu\text{m}$, $a = 1.71 \mu\text{m}$, $R_a = 200 \Omega\text{cm}$; $l = 1,265 \mu\text{m}$, $a = 1.36 \mu\text{m}$, $R_a = 100 \Omega\text{cm}$; $l = 1,594 \mu\text{m}$, $a = 1.08 \mu\text{m}$, $R_a = 50 \Omega\text{cm}$).

from 5 to 50 nS (Pongracz et al. 1991; Stefani and Steinbach 1969; Stratford et al. 1989).

Another observation that should be noted from the data in Fig. 7 and Table 2 is that the difference between the microelectrode and patch-clamp estimates of R_N and τ_0 are larger for granule neurons than for CA1 or CA3 pyramidal neurons. Granule neurons also display a larger discrepancy in the effects of a leak on R_N and τ_0 . One possible reason for these differences is that a fixed microelectrode leak conductance would have a greater effect on the measured R_N of granule neurons than on the larger pyramidal neurons.

DISCUSSION

Comparison of patch-clamp and microelectrode results

The results of this study indicate that both R_N and τ_0 for all three classes of hippocampal neurons are larger than previously determined by the use of conventional microelectrode techniques. This finding is consistent with the results of others who have reported that patch-clamp methods yield larger R_N and slower τ_0 values than microelectrode recordings (Blanton et al. 1989; Coleman and Miller 1989; Edwards et al. 1989).

Can the presence of a somatic leak account for the differences in patch-clamp and microelectrode data?

The two most obvious explanations for the disparity of the data obtained with patch-clamp and microelectrode recordings are the leak conductance introduced by microelectrode impalement and the dialysis of the cytoplasm by the contents of patch-clamp electrodes. The use of perforated patch-clamp recordings to eliminate the dialysis problem suggests that the larger values of R_N and τ_0 are a consequence of the absence of a microelectrode-induced leak conductance in these recordings. Two observations need to be reconciled with this explanation, however: patch-clamp recordings yield R_N values that are disproportionately large compared with τ_0 , and there is no obvious difference between the resting potential of patch-clamp and microelectrode recordings.

In all three classes of hippocampal neurons, the R_N values obtained with patch-clamp recording are larger relative to those obtained in microelectrode recordings than are the τ_0 values (see Table 2). This observation suggests that microelectrode penetration may have a larger effect on the measured value of R_N than τ_0 . Although this result may not be intuitive, the results of both analytic and numerical models indicate that it can be explained by existing theoretical formulations of the effects of a somatic leak on R_N and τ_0 in equivalent cable models of neurons with extensive cable structures.

Despite the large differences in R_N and τ_0 obtained by the use of patch-clamp and microelectrode recordings, no obvious differences were observed in the resting potentials measured with the use of these methods. For a leak conductance to result in more depolarized resting potentials, at least two conditions would have to be met: the leak induced by microelectrode impalement would have to have a reversal potential depolarized to rest, and there would have to be no com-

ensation for the leak by electrogenic pumps, voltage- and/or Ca^{2+} -dependent conductances, or redistribution of ions (see Clements and Redman 1989; Fleshman et al. 1988 for discussion). The fact that a somatic leak accounts well for the differences in R_N and τ_0 observed with patch-clamp and microelectrode recordings suggests that one or a combination of the above mechanisms is likely to maintain resting potentials at negative values in the presence of a microelectrode-induced leak conductance (see also Pongracz et al. 1991).

Interpretation of τ_0 as τ_m and estimation of membrane resistivity

Theoretically, passive charging of the membrane in response to a current step should have a time course described by an infinite sum of exponentials (Rall 1969), with the slowest time constant (τ_0) being the membrane time constant (τ_m). The equivalence of τ_0 and τ_m holds only if the membrane resistivity (R_m) is uniform. If a microelectrode-induced somatic leak is present, or if the dendritic terminations are leaky or short circuited, this assumption does not hold, and τ_0 does not provide an accurate estimate of τ_m . If the membrane is assumed to have uniform R_m , and a passive component of the voltage response to a step of current is functionally defined and identified (see criteria outlined in METHODS), τ_0 can be interpreted as a reasonable estimate of the membrane time constant (τ_m).

The membrane resistivity (R_m) can be estimated from the definition of τ_m , $\tau_m = R_m C_m$. Because a value of $1.0 \mu\text{F}/\text{cm}^2$ is generally assumed for C_m (Brown et al. 1981b; Cole 1968), the τ_m values estimated from measurements of τ_0 in this study correspond to R_m values of $28,000 \Omega\text{cm}^2$ for CA1 pyramidal neurons, $66,000 \Omega\text{cm}^2$ for CA3 pyramidal neurons, and $43,000 \Omega\text{cm}^2$ for dentate granule neurons. Although C_m is thought to be constant for biological membranes, this assumption is based on data from a limited set of preparations (see Brown et al. 1981b for discussion). C_m values different from $1.0 \mu\text{F}/\text{cm}^2$ would imply that R_m is different from the values given above.

Perforated patch-clamp recordings eliminate the somatic leak and therefore provide more accurate estimates of τ_m from τ_0 than do microelectrode recordings. Nevertheless, it is possible that physiological nonuniformities in R_m exist, and consequently estimates of τ_m based on measurements of τ_0 would be inaccurate. The effect of such nonuniformities in R_m would be to render R_m a spatially weighted average of R_m in different regions of the neuron.

Does the higher membrane resistivity imply that hippocampal neurons are isopotential?

The improved estimates of R_m provided by perforated patch-clamp recordings may have important implications for the integration of synaptic input in hippocampal neurons, but the data do not suggest that hippocampal neurons are isopotential. In fact, the results obtained with the equivalent cylinder models suggest that the disproportionate differences in R_N and τ_0 estimates provided by patch-clamp and microelectrode recordings can only be explained if hip-

hippocampal neurons have substantial electrotonic lengths. Data from dentate granule neurons, for example, are best fit with an equivalent cylinder model having an electrotonic length of 0.74. This should only be considered a rough estimate of L , however, because it is based on data from a sample with large variability in the parameters measured, and because granule neurons have a large degree of morphological variability (Claiborne et al. 1990). Nevertheless, the present data, combined with the modeling results, strongly suggest that hippocampal neurons have significant electrotonic lengths despite the large R_N and τ_0 values measured in the absence of a somatic leak.

Although dentate granule neurons may be reasonably represented by a single equivalent cylinder attached to a soma (Turner and Schwartzkroin 1983), it is likely that more complex representations are necessary for CA1 and CA3 pyramidal neurons. In particular, tapering of the proximal dendrites and termination of the apical and basal dendritic trees of pyramidal neurons at different electrotonic lengths appear to represent significant deviations from the morphological requirements for an equivalent cylinder representation (Stratford et al. 1989; Turner and Schwartzkroin 1983). Because of the variability of physiological and morphological parameters within populations of neurons, accurate estimates of the cable properties of these neurons will require paired physiological and morphological data from the same neurons. Nevertheless, our data suggest that, despite the high membrane resistivity, hippocampal neurons are not isopotential and have electrotonic structures that are likely to play an important role in synaptic integration. Another point worthy of note is that the nonisopotentiality of these neurons poses a substantial barrier to the ability to adequately voltage clamp synaptic and voltage-gated conductances in the dendrites. Errors associated with conductance and kinetic measurements from hippocampal neurons can be considerable unless the channels underlying the measured currents are electrotonically close to the soma (Brown and Johnston 1983; Johnston and Brown 1983).

Physiological basis of passive membrane properties

A very important neurophysiological question that remains to be addressed is what ion channels determine the membrane properties of neurons? Is membrane resistivity determined primarily by voltage-dependent channels open near the resting potential or by passive channels that are open at all potentials? Although our data do not address this issue directly, they do provide some insight into the matter.

We have focused our efforts on accurately determining R_N and τ_0 near the resting membrane potential in the three major classes of hippocampal neurons. Because by definition passive membrane properties should not be measured under conditions where voltage-dependent conductances are active (Rall 1977), we used the criteria described in METHODS to avoid errors resulting from activation of voltage-dependent conductances by the current step. If these criteria are applied, only very small voltage responses (<10 mV) could be considered passive, with larger responses showing signs of activation of voltage-dependent conductances. Accordingly, changing the membrane potential

with steady current injection resulted in significant differences in passive membrane properties. This finding suggests that voltage-dependent conductances active near the resting potential provide a substantial contribution to the measured values of R_N and τ_0 . The nature of these voltage-dependent conductances is not clear, although our data indicate that there are differences among the three classes of neurons, suggesting that different types, densities, and distributions of voltage-gated channels are active at rest in each class of hippocampal neurons.

In all three classes of neurons, both R_N and τ_0 were larger at more depolarized potentials. This type of membrane rectification was first described in muscle (Adrian and Freygang 1962; Katz 1949) and later in invertebrate neurons (Kandel and Tauc 1966), spinal motoneurons (Ito and Oshima 1965; Nelson and Frank 1967), and hippocampal CA1 pyramidal neurons (Hotson et al. 1979). An increased R_N at depolarized potentials (or anomalous rectification, as it has been called) can theoretically arise because of a conductance activated by hyperpolarization that decreases membrane resistivity at hyperpolarized potentials or because of an inward current activated by depolarization that increases the size of a response to depolarizing current injections.

The slowly inactivating Na^+ current (French and Gage 1985; Stafstrom et al. 1982) or the T-type Ca^+ current (Fisher et al. 1990; Nowycky et al. 1985) have properties that could increase the voltage response to small depolarizing current injections and produce an apparent increase in R_N at depolarized potentials. Indeed, the increased R_N observed by Hotson et al. at depolarized potentials in CA1 pyramidal neurons was blocked by Mn^{2+} or tetrodotoxin (TTX) and enhanced by Ba^{2+} , suggesting that this rectification is caused by activation of low-threshold Na^+ and/or Ca^{2+} currents (Hotson et al. 1979). The reversal of the rectification we observed in CA1 neurons after application of 2–5 mM Cs^+ , however, suggests that Cs^+ -sensitive conductances also contribute to the rectification.

Currents activated by hyperpolarization generally fall into three categories: inward-rectifying K^+ currents, mixed cation (Na^+/K^+) currents, and Cl^- currents. Inward-rectifying K^+ currents have been described in muscle (Stanfield 1970), starfish eggs (Hagiwara et al. 1976), tunicate eggs (Ohmori 1978), cortical neurons (Constanti and Galvan 1983), and hippocampal neurons (Grove and Halliwell 1990; Owen 1987). These conductances are partially active at potentials as positive as -60 mV in hippocampal neurons (Owen 1987) but can only be detected as a depolarizing sag at potentials negative to the equilibrium potential for K^+ . Also, the negative reversal potential of this current results in an asymmetry of the current-on and current-off voltage responses, with the depolarizing sag seen only in the hyperpolarizing voltage response (Constanti and Galvan 1983). Mixed cation currents activated by hyperpolarization were first described in cardiac muscle (Brown and DiFrancesco 1980; DiFrancesco 1981; DiFrancesco et al. 1986; Yanagihara and Irisawa 1980) and later in hippocampal and cortical neurons (Halliwell and Adams 1982; Spain et al. 1987). In contrast to the inward-rectifying K^+ current, the mixed cation current has a more depolarized reversal potential

resulting in symmetrical current-on and current-off voltage responses. Cl^- currents activated by hyperpolarization have also been described in *Aplysia* neurons (Chesnoy-Marchais 1983; Chesnoy-Marchais and Evans 1986), sympathetic neurons (Selyanko 1984), and hippocampal neurons (Madison et al. 1986).

The sensitivity of the sag to Cs^+ suggests that either an inward-rectifying K^+ current or a mixed cation current activated by hyperpolarization is responsible for the sag in hippocampal neurons (Constanti and Galvan 1983; Hagiwara et al. 1976; Halliwell and Adams 1982; Spain et al. 1987). In CA1 neurons, the symmetry of the voltage responses to hyperpolarizing current injections suggests that the sag is mediated by a mixed cation current activated by hyperpolarization. By contrast, voltage responses in CA3 pyramidal neurons and dentate granule neurons are less symmetrical, suggesting that either an inward-rectifying K^+ current or a different density or distribution of mixed cation channels is responsible for the sag in these neurons.

The reversal of the voltage dependence of R_N and τ_0 by Cs^+ in CA1 neurons suggests that the mixed cation current underlying the sag contributes significantly to the voltage dependence of R_N and τ_0 in these neurons. A second conductance (such as an outward-rectifying K^+ current; e.g., M-current or A-current) is likely to underlie the reversed voltage dependence of R_N and τ_0 observed in the presence of Cs^+ . In CA3 neurons, Cs^+ -sensitive conductances seem to be active at the resting potential and provide a significant contribution to R_N and τ_0 . The inability of Cs^+ to reverse the voltage dependence of R_N and τ_0 in CA3 pyramidal neurons or dentate granule neurons, however, suggests that Cs^+ -insensitive conductances (perhaps the Cl^- current activated by hyperpolarization, the slow Na^+ current, or a T-type Ca^{2+} current) primarily determine the membrane rectification in these neurons.

All three of the currents activated by hyperpolarization have been reported to be active at or near normal resting potentials (Halliwell and Adams 1982; Madison et al. 1986; Owen 1987; Spain et al. 1987). In addition, a number of other ion channels active at rest have been described in a variety of neurons. Some of these, such as the slowly inactivating (delay) K^+ current (Storm 1990), the muscarinic K^+ current (Brown 1988; Brown et al. 1990), the low-threshold Na^+ current (French and Gage 1985; Stafstrom et al. 1982), and the T-type Ca^+ current (Fisher et al. 1990), are voltage dependent, whereas others, such as a second class of muscarinic K^+ current (Benson et al. 1988; Madison et al. 1987), some muscarine-insensitive K^+ currents (Jones 1989; Storm 1990), and a number of Cl^- currents (Franciolini and Nonner 1987; Franciolini and Petris 1988; Owen et al. 1988), are voltage insensitive or weakly voltage dependent. The extent to which each of these currents contributes to R_N and τ_0 and the voltage dependence of these parameters in hippocampal neurons remains to be determined. It is clear, however, that the so-called passive membrane properties of hippocampal neurons are determined at least in part by voltage-dependent conductances open at the resting potential and that different densities and/or distributions of these conductances are likely to determine R_m for each class of hippocampal neuron.

In addition to voltage-gated channels, background synaptic activity or activation of ligand-gated channels by ambient levels of neurotransmitters in cerebrospinal fluid may provide a significant contribution to R_m (Barrett 1975; Bernander et al. 1991). Furthermore, nonuniform synaptic input or nonuniform distribution of voltage- or ligand-gated channels may result in regional differences in R_m within the dendritic trees of individual neurons. The functional consequences of such nonuniformities have been analyzed and discussed in detail by Holmes and Woody (1989).

Differences among classes of neurons in the hippocampus

The values for R_m determined in this study represent substantial increases over previous estimates of R_m derived from microelectrode studies (see Fig. 7; granule neurons, 3.5-fold increase; CA3 neurons, 2.8-fold increase; CA1 neurons, 1.9-fold increase). This suggests that microelectrode impalement may have a larger effect on the measured membrane properties of dentate granule neurons than pyramidal neurons, presumably because the somata of granule cells are smaller. Both the perforated patch-clamp data and the microelectrode data indicate that R_m is largest for CA3 pyramidal neurons. In contrast to microelectrode data, however, the patch-clamp data indicate that R_m is larger for granule neurons than for CA1 neurons. The differences among all three classes of neurons are all statistically significant (1-factor ANOVA with Tukey's test for multiple comparisons; $q = 11.089$ for CA1 and CA3; $q = 4.295$ for CA1 and dentate; $q = 6.632$ for CA3 and dentate).

The implications for the differences in R_m among the three classes of neurons in the hippocampus are unclear. It has been suggested that such differences may serve to match the R_N values of cells with dramatically different morphologies (Brown et al. 1981a). This could be the case for CA1 and CA3 pyramidal neurons, which this study suggests have very similar values for R_N despite the differences in R_m and morphology. This appears not to be the case for granule neurons, however, which this study suggests have statistically larger R_N values than both CA1 and CA3 pyramidal neurons (1-factor ANOVA with Tukey's test for multiple comparisons; $q = 6.896$ and 6.499, respectively).

Functional implications of higher membrane resistivity

The most obvious functional implication of the higher membrane resistivity is reflected in the higher input resistances measured with patch-clamp recording. Because the lower estimates of R_m provided by microelectrode recordings are generally assumed to reflect uniform somatic and dendritic membrane properties, this leads to artificially low estimates of input resistances, not only at the soma, but also at the site of synapses in the dendritic tree and on spine heads. The higher estimates of R_m measured in the absence of a somatic leak are likely to be much closer to reality for dendritic membrane even if physiological nonuniformities in R_m exist in neurons. Thus the higher membrane resistivity suggested by patch-clamp data implies that the change in membrane potential in response to a small current at any given point on the neuron will be larger than previously believed.

The higher membrane resistivity will also affect the time course of the decay of membrane potential. Because synaptic potentials ideally decay according to the membrane time constant (but see Williams and Johnston 1991), larger values of τ_m imply that synaptic potentials actually decay much slower than was believed on the basis of microelectrode estimates of τ_m . This has significant implications for processes such as temporal summation and spike accommodation.

The larger estimates of membrane resistivity also affect the attenuation of synaptic potentials in the dendritic tree. Our data, in combination with modeling of microelectrode data by the addition of a microelectrode leak, can only be explained if hippocampal neurons have significant electrotonic lengths. Consequently, it is likely that, despite the high R_m indicated by patch-clamp recordings, synaptic and voltage-activated potentials decay substantially as they propagate passively from the dendrites to the soma or vice versa. Furthermore, it should be noted that electrotonic decay would be greatest for rapid events such as fast synaptic and voltage-activated potentials. The cable properties of hippocampal neurons certainly need to be reevaluated in light of the fact that previous analyses were based on voltage responses that were influenced by impalement-induced leak conductances.

Finally, our data indicate that the passive membrane properties of hippocampal neurons are determined, at least in part, by voltage-dependent conductances active at the resting potential, and that the types, densities, and distributions of channels underlying these properties differ among the three major classes of hippocampal neurons. Others have shown that regenerative Na^+ and Ca^{2+} conductances are also localized in the dendrites (Huguenard et al. 1989; Traub and Llinás 1979; Turner et al. 1991; Wong et al. 1979) and that background synaptic activity can influence the cable properties of neurons (Barrett 1975; Bernander et al. 1992). All of these conductances are likely to play an important role in integration of synaptic input in the dendritic trees of hippocampal neurons. Furthermore, evidence that many of these conductances may be modulated by neurotransmitters (for reviews, see Brown et al. 1990; Storm 1990) opens up the further interesting complication that passive membrane properties are not likely to be constants as they are usually described, but vary according to the state of a neuron as it receives thousands of synaptic and neuromodulatory inputs from other neurons in the brain.

APPENDIX

To determine the theoretical effects of introducing a leak conductance at the soma, an analytic model of an equivalent cylinder attached to a lumped soma was derived from previously published equations (Durand 1984; Iasek and Redman 1973; Kawato 1984; Poznański 1987a,b; Rall 1977). Model simulations were performed with the use of *Mathematica*, running on a NeXT computer (68030 microprocessor; NeXTstep 2.0; Mach, UNIX).

Glossary

A_s	surface area of the soma
a	cable radius

G_s	somatic conductance
I	current injection
L	electrotonic length
l	cable length
R_a	axial resistivity
$R_{m(d)}$	dendritic membrane resistivity
$R_{m(s)}$	somatic membrane resistivity
R_N	input resistance
r	soma radius
t	time
$V(0, t)$	voltage at the soma at time t
$V(0, \infty)$	voltage at the soma in the steady state
α_n	n th root of transcendental Eqs. A6 and A13
β	ratio of dendritic-to-somatic membrane resistivity
λ	space constant of the cable
ρ	dendritic-to-somatic conductance ratio
ρ_∞	dendritic-to-somatic conductance ratio for an infinite cable with $R_{m(s)} = R_{m(d)}$
ρ^*	dendritic-to-somatic conductance ratio for an infinite cable with $R_{m(s)} < R_{m(d)}$
τ_m	membrane time constant
$\tau_{m(d)}$	dendritic membrane time constant
$\tau_{m(s)}$	somatic membrane time constant
τ_n	n th time constant in the series

Analytic solutions of equivalent cylinder models

Analytic solutions for the cable equations with a leak conductance at the soma were first published by Iasek and Redman (1973). Their derivation was for the case of an infinitely long one-dimensional cable connected to a lumped soma. They introduced the term β to describe the somatic leak, which is defined as the ratio of the dendritic membrane resistivity to the somatic membrane resistivity

$$\beta = R_{m(d)}/R_{m(s)} \quad (A1)$$

The derivation for the transient voltage response to a step of current was later extended to the case of a finite cable attached to a lumped soma (Durand 1984; Kawato 1984; Poznański 1987a,b). The finite cable model is characterized by the electrotonic length of the cable (L) and the dendritic-to-somatic conductance ratio (ρ). Kawato introduced the term ρ^* , which is related to ρ_∞ by the following expression

$$\rho^* = \beta\rho_\infty \quad (A2)$$

Physically, ρ_∞ is the dendritic-to-somatic conductance ratio for the infinite cable with uniform membrane resistivity, $R_{m(d)}$, attached to a soma with a lower membrane resistivity, $R_{m(s)}$. ρ^* corresponds to the dendritic-to-somatic conductance ratio for an equivalent cylinder and soma with uniform R_m equal to $R_{m(d)}$.

When a leak conductance is present at the soma (i.e., $\beta > 1$), the voltage at the soma, in response to a step of current at the soma, is described by a sum of exponentials

$$V(0, t) = V(0, \infty) - \sum_{n=0}^{\infty} C_n e^{-t/\tau_n} \quad (A3)$$

where both the coefficients (C_n) and the time constants (τ_n) are functions of β , and the steady-state voltage, $V(0, \infty)$, is given by the product of the current injected (I) and the input resistance (R_N)

$$V(0, \infty) = IR_N \quad (A4)$$

The time constants in Eq. A3 can be determined from the equation

$$\tau_n = \frac{\tau_{m(d)}}{(1 + \alpha_n^2)} \quad (A5)$$

where $\tau_{m(d)}$ is the dendritic membrane time constant, and α_n are the roots of the following transcendental equation

$$\tan(\alpha_n L) = \frac{\beta - (1 + \alpha_n^2)}{\alpha_n \rho^*} \quad (A6)$$

The first time constant in this series (τ_0 ; $\alpha_0 = 0$) falls between the dendritic membrane time constant [$\tau_{m(d)}$] and the somatic membrane time constant [$\tau_{m(s)}$]. The coefficients in Eq. A3 are determined from the following expression

$$C_n = \frac{2I\beta\rho^*\alpha_n^2}{G_s(1 + \alpha_n^2)[(-1 - \alpha_n^2 + \beta)^2 L + \alpha_n^2 \rho^* + (-1 + \beta)\rho^* + \alpha_n^2 L\rho^{*2}]} \quad (A7)$$

Model simulations were run for cables of varying l , a , and R_a attached to spherical somata with varying r and varying $R_{m(s)}$. The somatic conductance (G_s) was determined by the equation

$$G_s = \frac{A_s}{R_{m(d)}/\beta} \quad (A8)$$

where A_s is the surface area of the soma ($A_s = 4\pi r^2$ for a sphere). Input resistance (R_N) was determined from the equation

$$R_N = \frac{1}{G_s(1 + \rho)} \quad (A9)$$

where ρ is the dendritic-to-somatic conductance ratio for a finite cable and is determined from the equations

$$\rho_\infty = \frac{\pi a^2}{\lambda R_a G_s} \quad (A10)$$

$$\rho = \tanh(L)\rho_\infty = \tanh(L)\rho^*/\beta \quad (A11)$$

and λ is the space constant of the cable

$$\lambda = \sqrt{\frac{aR_m}{2R_a}} \quad (A12)$$

Solutions for the first three roots of Eq. A5 were determined with the use of *Mathematica*, which provides a computerized implementation of Newton's method for finding the roots of transcendental equations. The values for $\alpha_{0,1,2}$ were then used to determine $\tau_{0,1,2}$ from Eq. A5 and $C_{0,1,2}$ from Eq. A7. These values were then used to generate voltage responses from the first three terms in the series in Eq. A3. The values of R_N and τ_0 were determined empirically from the voltage responses by the use of the same methods described for experimental data (see METHODS). The empirical values for R_N and τ_0 were in perfect agreement with the analytic values determined from Eqs. A5 and A9.

The effects of changing β on R_N and τ_0 are shown for various models in Figs. 8 and 9 and discussed in the text. All R_N and τ_0 values determined in the model are normalized to the values for the case where there is no somatic leak [i.e., $R_{m(d)} = R_{m(s)}$] and expressed as $R_N(\beta)/R_N(1)$ and $\tau_0(\beta)/\tau_0(1)$. Because Eq. A7 has no solution when $\beta = 1$ and $\alpha_0 = 0$, the time constants and coefficients for Eq. A3 were calculated with the use of the equations published by Rall for a uniform cable attached to a soma with identical membrane properties (Rall 1977). The time constants are determined from Eq. A5, with the only difference being that α_n is the n th root of the following transcendental equation

$$\alpha_n L \cot(\alpha L) = -\rho L \coth(L) = -k \quad (A13)$$

The first coefficient of Eq. A3 is given by

$$C_0 = V(0, \infty) \left(\frac{\rho + 1}{k + 1} \right) \quad (A14)$$

and subsequent coefficients are given by the following equation

$$C_n = \frac{2C_0\tau_n/\tau_0}{[1 + (\alpha_n L)^2]/(k^2 + k)} \quad (A15)$$

Numerical simulations of compartmental models

As an independent test of the results obtained with the analytic model described in the previous section, numerical simulations of voltage responses were computed with the use of CABLE, a program for numerically solving the cable equations for neurons with arbitrary branching geometries (Hines 1989). All simulations in CABLE were run on a Solbourne Series 5 computer (Sun-4 compatible SPARC station; Sun OS/SMP 4.0).

Neurons consisting of a finite equivalent cylinder attached to a lumped soma were modeled with the use of a single compartment to represent the soma and up to 100 compartments arranged linearly to represent the equivalent cylinder. The number of compartments used to model the equivalent cylinder was chosen so that no one compartment was ever larger than 0.2λ . This criterion for compartment size has been reported to yield accurate numerical simulations in compartmental models of neurons with complicated branching morphologies (Segev et al. 1985). The numerical equivalent cylinder models provided an independent confirmation of the analytic models, because the data shown in Figs. 8 and 9 could be reproduced in numerical simulations with the use of compartmental representations of equivalent cylinder models.

We thank D. Jaffe and S. Williams for helpful discussion. We also thank B. Claiborne for providing unpublished data on granule neuron morphology, S. Williams and A. Nobre for helpful suggestions on the manuscript, R. Gray for technical assistance, and M. Haque for computer assistance. This work was supported by National Institutes of Health Grants NS-11535 and MH-44754, and Air Force Office of Scientific Research, 88-0142.

Address for reprint requests: D. Johnston, Division of Neuroscience, Baylor College of Medicine, One Baylor Plaza, Houston, TX 77030.

Received 13 May 1991; accepted in final form 22 October 1991.

REFERENCES

- ADRIAN, R. H. AND FREYGANG, W. H. The potassium and chloride conductance of frog muscle membrane. *J. Physiol. Lond.* 163: 61–103, 1962.
- BARRETT, J. N. Motoneuron dendrites: role in synaptic integration. *Federation Proc.* 34: 1398–1407, 1975.
- BARRETT, J. N. AND CRILL, W. E. Specific membrane properties of cat motoneurons. *J. Physiol. Lond.* 239: 301–324, 1974.
- BENSON, D. M., BLITZER, R. D., AND LANDAU, E. M. An analysis of the depolarization produced in guinea-pig hippocampus by cholinergic receptor stimulation. *J. Physiol. Lond.* 404: 479–496, 1988.
- BERNANDER, O., DOUGLAS, R. J., MARTIN, K. A. C., AND KOCH, C. Synaptic background activity determines spatio-temporal integration in single pyramidal cells. *Proc. Natl. Acad. Sci. USA* 88:11569–11573, 1991.
- BLANTON, M. G., LOTURCO, J. J., AND KRIEGSTEIN, A. R. Whole cell recording from neurons in slices of reptilian and mammalian cerebral cortex. *J. Neurosci. Methods* 30: 203–210, 1989.
- BROWN, D. M-currents: an update. *Trends Neurosci.* 11: 294–299, 1988.
- BROWN, D. A., GÄHWILER, B. H., GRIFFITH, W. H., AND HALLIWELL, J. V. Membrane currents in hippocampal neurons. *Prog. Brain Res.* 83: 141–160, 1990.
- BROWN, H. F. AND DI FRANCESCO, D. Voltage-clamp investigations of membrane currents underlying pacemaker activity in rabbit sino-atrial node. *J. Physiol. Lond.* 308: 331–351, 1980.
- BROWN, T. H., FRICKE, R. A., AND PERKEL, D. H. Passive electrical constants in three classes of hippocampal neurons. *J. Neurophysiol.* 46: 812–827, 1981a.
- BROWN, T. H. AND JOHNSTON, D. Voltage-clamp analysis of mossy fiber synaptic input to hippocampal neurons. *J. Neurophysiol.* 50: 487–507, 1983.
- BROWN, T. H., PERKEL, D. H., NORRIS, J. C., AND PEACOCK, J. H. Electrotonic structure and specific membrane properties of mouse dorsal root ganglion neurons. *J. Neurophysiol.* 45: 1–15, 1981b.
- CARNEVALE, N. T. AND JOHNSTON, D. Electrophysiological characterization of remote chemical synapses. *J. Neurophysiol.* 47: 606–621, 1982.
- CHESNOY-MARCHELIS, D. Characterization of a chloride conductance activated by hyperpolarization in *Aplysia* neurones. *J. Physiol. Lond.* 342: 277–308, 1983.
- CHESNOY-MARCHELIS, D. AND EVANS, M. G. Chloride channels activated by hyperpolarization in *Aplysia* neurones. *Pfluegers Arch.* 407: 694–696, 1986.
- CLAIBORNE, B. J., AMARAL, D. G., AND COWAN, W. M. Quantitative, three-dimensional analysis of granule cell dendrites in the rat dentate gyrus. *J. Comp. Neurol.* 302: 206–219, 1990.
- CLEMENTS, J. D. AND REDMAN, S. J. Cable properties of cat spinal motoneurons measured by combining voltage clamp, current clamp and intracellular staining. *J. Physiol. Lond.* 409: 63–87, 1989.
- COLE, K. S. In: *Membranes, Ions, and Impulses*. Berkeley, CA: Univ. of California Press, 1968.
- COLEMAN, P. A. AND MILLER, R. F. Measurement of passive membrane parameters with whole-cell recording from neurons in intact amphibian retina. *J. Neurophysiol.* 61: 218–230, 1989.
- CONSTANTI, A. AND GALVAN, M. Fast inward-rectifying current accounts for anomalous rectification in olfactory cortex neurones. *J. Physiol. Lond.* 335: 153–178, 1983.
- DI FRANCESCO, D. A new interpretation of the pace-maker current in calf Purkinje fibres. *J. Physiol. Lond.* 314: 359–376, 1981.
- DI FRANCESCO, D. Block and activation of the pace-maker channel in calf Purkinje fibres: effects of potassium, caesium, and rubidium. *J. Physiol. Lond.* 329: 485–507, 1982.
- DI FRANCESCO, D., FERRONI, A., MAZZANTI, M., AND TROMBA, C. Properties of the hyperpolarizing-activated current (i_f) in cells isolated from the rabbit sino-atrial node. *J. Physiol. Lond.* 377: 61–88, 1986.
- DI FRANCESCO, D. AND OJEDA, C. Properties of the current i_f in the sino-atrial node of the rabbit compared with those of the current i_{k2} in Purkinje fibre. *J. Physiol. Lond.* 308: 353–367, 1980.
- DURAND, D. The somatic shunt cable model for neurons. *Biophys. J.* 46: 645–653, 1984.
- DURAND, D., CARLEN, P. L., GUREVICH, N., HO, A., AND KUNOV, H. Electrotonic parameters of rat dentate granule cells measured using short current pulses and HRP staining. *J. Neurophysiol.* 50: 1080–1097, 1983.
- EDWARDS, F. A., KONNERTH, A., SAKMANN, B., AND TAKAHASHI, T. A thin slice preparation for patch clamp recordings from neurones of the mammalian central nervous system. *Pfluegers Arch.* 414: 600–612, 1989.
- FATT, P. Electric potentials occurring around a neurone during its antidromic activation. *J. Neurophysiol.* 20: 27–60, 1957.
- FISHER, R. E., GRAY, R., AND JOHNSTON, D. Properties and distribution of single voltage-gated calcium channels in adult hippocampal neurons. *J. Neurophysiol.* 64: 91–104, 1990.
- FLESHMAN, J. W., SEGEV, I., AND BURKE, R. E. Electrotonic architecture of type-identified α -motoneurons in the cat spinal cord. *J. Neurophysiol.* 60: 60–85, 1988.
- FRANCIOLINI, F. AND NONNER, W. Anion and cation permeability of a chloride channel in rat hippocampal neurons. *J. Gen. Physiol.* 90: 453–478, 1987.
- FRANCIOLINI, F. AND PETRIS, A. Single chloride channels in cultured rat neurones. *Arch. Biochem. Biophys.* 261: 97–102, 1988.
- FRENCH, C. R. AND GAGE, P. W. A threshold sodium current in pyramidal cells in rat hippocampus. *Neurosci. Lett.* 56: 289–293, 1985.
- GROVE, E. A. AND HALLIWELL, J. V. Two inward rectifier currents revealed in CA1 neurones of the rat hippocampus in vitro (Abstract). *J. Physiol. Lond.* 424: 46P, 1990.
- HAGIWARA, S., MIYAZAKI, S., AND ROSENTHAL, N. P. Potassium current and the effect of cesium on this current during anomalous rectification of the egg cell membrane of a starfish. *J. Gen. Physiol.* 67: 621–638, 1976.
- HALLIWELL, J. V. AND ADAMS, P. R. Voltage-clamp analysis of muscarinic excitation in hippocampal neurones. *Brain Res.* 250: 71–92, 1982.
- HINES, M. A program for simulation of nerve equations with branching geometries. *Int. J. Biomed. Comput.* 24: 55–68, 1989.
- HOLMES, W. R. AND WOODY, C. D. Effects of uniform and non-uniform synaptic 'activation-distributions' on the cable properties of modeled cortical pyramidal neurons. *Brain Res.* 505: 12–22, 1989.
- HORN, R. AND MARTY, A. Muscarinic activation of ionic currents measured by a new whole-cell recording method. *J. Gen. Physiol.* 92: 145–159, 1988.
- HOTSON, J. R., PRINCE, D. A., AND SCHWARTZKROIN, P. A. Anomalous inward rectification in hippocampal neurons. *J. Neurophysiol.* 42: 889–895, 1979.
- HUGUENARD, J. R., HAMIL, O. P., AND PRINCE, D. A. Sodium channels in dendrites of rat cortical pyramidal neurons. *Proc. Natl. Acad. Sci. USA* 86: 2473–2477, 1989.
- IANSEK, R. AND REDMAN, S. J. An analysis of the cable properties of spinal motoneurons using a brief intracellular current pulse. *J. Physiol. Lond.* 234: 613–636, 1973.
- ITO, M. AND OSHIMA, T. Electrical behaviour of the motoneurone membrane during intracellularly applied current steps. *J. Physiol. Lond.* 180: 607–635, 1965.
- JACK, J. An introduction to linear cable theory. In: *The Neurosciences Fourth Study Program*, edited by F. O. Schmitt and F. G. Worden. Cambridge, MA: MIT Press, 1979, p. 423–437.
- JACK, J. J. B. AND REDMAN, S. J. An electrical description of the motoneurone, and its application to the analysis of synaptic potentials. *J. Physiol. Lond.* 215: 321–352, 1971.
- JOHNSTON, D. Passive cable properties of hippocampal CA3 pyramidal neurons. *Cell. Mol. Neurobiol.* 1: 41–55, 1981.
- JOHNSTON, D. AND BROWN, T. H. Interpretation of voltage-clamp measurements in hippocampal neurons. *J. Neurophysiol.* 50: 464–486, 1983.
- JONES, S. W. On the resting potential of isolated frog sympathetic neurons. *Neuron* 3: 153–161, 1989.
- KANDEL, E. R. AND TAUC, L. Anomalous rectification in the metacerebral giant cells and its consequences for synaptic transmission. *J. Physiol. Lond.* 183: 287–304, 1966.
- KATZ, B. Les constantes électriques de la membrane du muscle. *Arch. Sci. Physiol.* 3: 285–299, 1949.
- KAWATO, M. Cable properties of a neuron model with non-uniform membrane resistivity. *J. Theor. Biol.* 111: 149–169, 1984.
- KORN, S. J. AND HORN, R. Influence of sodium-calcium exchange on calcium current rundown and the duration of calcium-dependent chloride currents in pituitary cells, studied with whole cell and perforated patch recording. *J. Gen. Physiol.* 94: 789–812, 1989.
- LORENTE DE NÓ, R. Studies on the structure of the cerebral cortex. II. Continuation of the study of the ammonic system. *J. Psychol. Neurol. Lpz.* 46: 113–177, 1934.

- MADISON, D. V., LANCASTER, B., AND NICOLL, R. A. Voltage clamp analysis of cholinergic action in the hippocampus. *J. Neurosci.* 7: 733-741, 1987.
- MADISON, D. V., MALENKA, R. C., AND NICOLL, R. A. Phorbol esters block a voltage-sensitive chloride current in hippocampal pyramidal cells. *Nature Lond.* 321: 695-697, 1986.
- NELSON, P. G. AND FRANK, K. Anomalous rectification in cat spinal motoneurons and effect of polarizing currents on excitatory postsynaptic potential. *J. Neurophysiol.* 30: 1097-1113, 1967.
- NOWYCKY, M. C., FOX, A. P., AND TSIEN, R. W. Three types of neuronal calcium channel with different calcium agonist sensitivity. *Nature Lond.* 316: 440-443, 1985.
- OHMORI, H. Inactivation kinetics and steady-state current noise in the anomalous rectifier of tunicate egg cell membranes. *J. Physiol. Lond.* 281: 77-99, 1978.
- OWEN, D. G. Three types of inward rectifier currents in cultured hippocampal neurons. *Neurosci. Lett. Suppl.* 29: S18, 1987.
- OWEN, D. G., HARRISON, N. L., AND BARKER, J. L. Three types of chloride channels in cultured rat hippocampal neurons. *Soc. Neurosci. Abstr.* 14: 1203, 1988.
- PONGRACZ, F., FIRESTEIN, S., AND SHEPHERD, G. M. Electrotonic structure of olfactory sensory neurons analyzed by intracellular and whole cell patch techniques. *J. Neurophysiol.* 65: 747-758, 1991.
- POZNAŃSKI, R. R. Transient response in a somatic shunt cable model for synaptic input activated at the terminal. *J. Theor. Biol.* 127: 31-50, 1987a.
- POZNAŃSKI, R. R. Techniques for obtaining analytical solutions for the somatic shunt cable model. *Math. Biosci.* 85: 13-35, 1987b.
- PROVENCER, S. W. A Fourier method for the analysis of exponential decay curves. *Biophys. J.* 16: 27-41, 1976.
- PURPURA, D. P., PRELEVIC, S., AND SANTINI, M. Hyperpolarizing increase in membrane conductance in hippocampal neurons. *Brain Res.* 7: 310-312, 1968.
- RALL, W. Branching dendritic trees and motoneuron membrane resistivity. *Exp. Neurol.* 1: 491-527, 1959.
- RALL, W. Time constants and electrotonic length of membrane cylinders and neurons. *Biophys. J.* 9: 1483-1508, 1969.
- RALL, W. Core conductor theory and cable properties of neurons. In: *Handbook of Physiology. The Nervous System. Cellular Biology of Neurons.* Bethesda, MD: Am. Physiol. Soc., 1977, sect. 1, vol. I, p. 39-97.
- REDMAN, S. J. The attenuation of passively propagating dendritic potentials in a motoneurone cable model. *J. Physiol. Lond.* 234: 637-664, 1973.
- REDMAN, S. J. A quantitative approach to integrative function of dendrites. In: *International Review of Physiology: Neurophysiology II*, edited by R. Porter. Baltimore, MD: University Park, 1976, vol. 10, p. 1-35.
- ROSE, P. K. AND VANNER, S. J. Differences in somatic and dendritic specific membrane resistivity of spinal motoneurons: an electrophysiological study of neck and shoulder motoneurons in the cat. *J. Neurophysiol.* 60: 149-166, 1988.
- SEGEV, I., FLESHMAN, J. W., MILLER, J. P., AND BUNOW, B. Modeling the electrical behavior of anatomically complex neurons using a network analysis program: passive membrane. *Biol. Cybern.* 53: 27-40, 1985.
- SELYANKO, A. A. Cd^{2+} suppresses a time-dependent Cl^- current in rat sympathetic neuron (Abstract). *J. Physiol. Lond.* 350: 49P, 1984.
- SHELTON, D. P. Membrane resistivity estimated for the Purkinje neuron by means of a passive computer model. *Neuroscience* 14: 111-131, 1985.
- SHERINGTON, C. S. In: *Integrative Action of the Nervous System.* New Haven, CT: Yale Univ. Press, 1906.
- SPAIN, W. J., SCHWINDT, P. C., AND CRILL, W. E. Anomalous rectification in neurons from cat sensorimotor cortex in vitro. *J. Neurophysiol.* 57: 1555-1576, 1987.
- STAFSTROM, C. E., SCHWINDT, P. C., AND CRILL, W. E. Negative slope conductance due to a persistent subthreshold sodium current in cat neocortical neurons in vitro. *Brain Res.* 236: 221-226, 1982.
- STANFIELD, P. R. The differential effects of tetraethyl-ammonium and zinc ions on the resting conductance of frog skeletal muscle. *J. Physiol. Lond.* 209: 231-256, 1970.
- STEFANI, E. AND STEINBACH, A. B. Resting potential and electrical properties of frog slow muscle fibres. Effect of different external solutions. *J. Physiol. Lond.* 203: 383-401, 1969.
- STORM, J. F. Potassium currents in hippocampal pyramidal cells. *Prog. Brain Res.* 83: 161-187, 1990.
- STRATFORD, K., MASON, A., LARKMAN, A., MAJOR, G., AND JACK, J. The modelling of pyramidal neurones in the visual cortex. In: *The Computing Neuron*, edited by R. Durbin, C. Miall, and G. Mitchinson. New York: Addison-Wesley, 1989, p. 296-321.
- TRAUB, R. D. AND LLINÁS, R. Hippocampal pyramidal cells: significance of dendritic ionic conductances for neuronal function and epileptogenesis. *J. Neurophysiol.* 42: 476-496, 1979.
- TURNER, D. A. AND SCHWARTZKROIN, P. A. Electrical characteristics of dendrites and dendritic spines in intracellularly stained CA3 and dentate hippocampal neurons. *J. Neurosci.* 3: 2381-2394, 1983.
- TURNER, R. W., MEYERS, D. E. R., RICHARDSON, T. L., AND BARKER, J. L. The site for initiation of action potential discharge over the somatodendritic axis of rat hippocampal CA1 pyramidal neurons. *J. Neurosci.* 11: 2270-2280, 1991.
- WILLIAMS, S. H. AND JOHNSTON, D. Kinetic properties of two anatomically distinct excitatory synapses in hippocampal CA3 neurons. *J. Neurophysiol.* 66: 1010-1020, 1991.
- WONG, R. K. S., PRINCE, D. A., AND BASBAUM, A. I. Intradendritic recordings from hippocampal neurons. *Proc. Natl. Acad. Sci. USA* 76: 986-990, 1979.
- YANAGIHARA, K. AND IRISAWA, H. Inward current activated during hyperpolarization in the rabbit sinoatrial node cell. *Pfluegers Arch.* 385: 11-19, 1980.